Multiband Fractal Antenna

By

Muhammad Waqas

2007-NUST-MS PhD-Elec-10

MSc 51(E)

Submitted to the Department of Electrical Engineering
In Partial Fulfillment of the requirements for the Degree of

Masters of Science
In
Electrical Engineering

Thesis Advisor
Dr. Mojeeb Bin Ihsan

College of Electrical & Mechanical Engineering
National University of Sciences & Technology
Rawalpindi, Pakistan
2009

ACKNOWLEDGMENTS

All praise is for Allah, the most beneficent and the most merciful.

First of all, I thank Allah Almighty for giving me the inspiration, patience, time, and strength to finish this work. With Allah's will and mercy I have been able to achieve all of this.

All thanks due especially to my family members, my father, mother, brothers and sisters for their prayers, and inspiration, which has helped me to stand where I am today.

It is my great pleasure to express my sincere appreciation and gratitude to my supervisor Dr. Mojeeb Bin Ihsan for guiding me and encouraging my work at each step of my thesis. His devotion to the needs of the students and the encouragements at each step has made working with him a true delight.

Special thanks and appreciation are due to my co-supervisor SRE Zubair Ahmad for his invaluable guidance and support at each step of my thesis. Without his support this thesis would not have been possible. I thank him for all his help and encouragements during my thesis work.

I would like to thank Dr. Khalid Munawar, Dr. Shahzad Amin Sheikh and SRE Zubair Ahmad for being in my Guidance and Examination Committee.

Dedicated to my Parents,

Brothers & Sisters

ABSTRACT

The booming progress of wireless systems and the recent development of a variety of wireless applications have remarkably increased the demand for multiband/wideband antennas. For example, car companies are looking to integrate systems such as AM, FM, GPS, GSM etc and at the same time maintain the good look of the vehicle. Traditionally different antennas were used for different frequency bands, which causes a limited space and place problem. Multiband antennas can be used to overcome this problem.

Most of the fractal geometries have self-similarity in their structure and recent research has shown that this self-similarity of fractals can be translated into its electromagnetic behavior. A fractal antenna based on the Sierpinski geometry is designed in this thesis that is capable of operating in multiple bands. The thesis involves design, simulation and fabrication of the Multiband Fractal antenna. The design and simulation of the antenna is carried out using FEM (Finite Element Method) and FITD (Finite Integral Time Domain) based electromagnetic simulators. Two different prototypes have been fabricated and tested. The measured results are compared with the corresponding simulated results, and good agreement is observed between both the results. The input impedance as well as input Return Loss shows a log-periodic behavior with a log-period of 2, the same scale factor that characterizes the Sierpinski Fractal geometry. The radiation patterns at these log-periodic bands also display good similarity. The geometrical scale factor of the Sierpinski fractal is changed and a monopole antenna based on this Perturbed Sierpinski fractal is designed and simulated. Band positions are changed according to the new scale factor but the bands are poorly matched. This poor input matching is improved by utilizing microstrip feed line. This Perturbed Sierpinski fed with microstrip line is fabricated and the measured results indicate that the band positions correspond to the new scale factor as well as the bands are well matched.

TABLE OF CONTENTS

LIST OF FIGURES

LIST OF TABLES

CHAPTER 1. INTRODUCTION

1.1 Brief Overview

A wireless system requires an antenna to radiate and receive electromagnetic waves. The antenna is therefore an essential component of a wireless system. With the rapid development in wireless communication systems and increasing importance of other wireless applications, multi-band/wideband antennas are in great demand, both for commercial and military applications. For example, car companies are looking to integrate systems such as AM, FM, GPS, GSM, UMTS and at the same time want to maintain the good look of the vehicle. Traditionally different antennas are used for different frequency bands, which causes a limited space and place problem. Multi-band antennas can be used to overcome this problem, where a single antenna can be used for different frequency bands.

Recent efforts in combining geometry with electromagnetic theory have resulted in the development of the rapidly growing field of fractal antenna engineering. Most of the fractals have self-similarity [1] in their structure and recent research [3] has shown that the self-similarity property of the fractal shapes can be translated into its electromagnetic behavior and result in a multi-band antenna.

Several fractal antennas geometries have been introduced and analyzed. One such example is Sierpinski Gasket type of fractal geometry, which has been used to design multiband monopole type antennas [10]. Several structures are derived from the original Sierpinski fractal structure and analyzed in order to get multi-band behavior [3], [18]. The monopole type Sierpinski antenna exhibits well-defined multi-band characteristics.

1.2 Objective

The main objectives of this thesis are:

- To get an understanding of the fractal antenna concept.
- To design, simulate and fabricate an antenna based on the Sierpinski fractal having the desired capability of multi-band operation.

- To carry out a comparative study of different variations of the classical Sierpinski monopole antenna.
- To improve the matching characteristics of the modified Sierpinski monopole antenna.

1.3 Motivation

- **Integration of multiple services:**

  With the advancement of wireless communications, several services need to be used. For example, today's automobile can have dozen of antennas that provide everything from emergency notification and navigational services to satellite radio and TV. Multiple antennas create performance challenges as well as aesthetic design issues.

- **Single Element rather than multiple elements:**

  Using fractal geometry, multi-band performance will be attained through the geometry of the conductor, rather than with the accumulation of separate elements that increase complexity and potential failure points. Multiple elements also cause a limited space and place problem.

1.4 Design Methodology

1.4.1 Sierpinski Fractal antenna Design

The design of Sierpinski Fractal Antenna is divided into two developments: software and hardware development.

1) **Software Development**
   - Design and Simulation with EM simulator, Ansoft HFSS
   - Simulated Return Loss
   - Simulated VSWR/ impedance bandwidth
   - Simulated Antenna radiation patterns
   - Simulated Antenna gain

2) **Hardware Development**

- PCB Fabrication
- Network Analyzer
- Anechoic chamber

After getting through the hardware development, both the simulated and measured results will be compared.

1.5 Thesis Organization

This thesis is organized into the following six chapters:

- **Chapter 1:** Introduction
- **Chapter 2:** Literature Survey
- **Chapter 3:** Design of Sierpinski monopole antenna
- **Chapter 4:** Variations of the Classical Sierpinski monopole antenna
- **Chapter 5:** Fabrication, Testing and Measurements
- **Chapter 6:** Results and Discussions

Chapter 1 gives a brief introduction of the thesis. It explains the objectives, motivation, and design methodology that has been used.

Chapter 2 summarizes the literature reviewed. It includes the basic fractal theory, key benefits of fractal-shaped antennas and some of the current research work carried out on fractal antennas.

Chapter 3 describes the main work of the thesis. It includes the design and simulation of the classical Sierpinski monopole antenna. The simulated results are also analyzed in this chapter. The last section of this chapter has the design and simulation of the fractal antenna for a practical application, that is, 2.4GHz / 5GHz Wireless LAN bands.

Chapter 4 discusses the different modifications of the classical Sierpinski monopole antenna. The simulated results are presented and compared with those of the classical Sierpinski monopole antenna in this chapter.

Chapter 5 describes the fabrication and testing of antennas that are designed and simulated. The measured results of the fabricated antennas are presented in this chapter.

Chapter 6 discusses the results of the antennas. Both the simulated as well as measured results are discussed here. Also a comparison between the measured results and simulated results is presented in this chapter.

CHAPTER 2. LITERATURE SURVEY

2.1 Introduction

This chapter presents a literature review of the theory of fractals and fractal-shaped antennas. An introduction to fractals along with their characteristic features is first discussed, elaborating with some classical examples. The generation of fractals is then discussed. Finally, the beneficial features of fractals in antenna design are presented and a review of research work carried out on fractal antennas is given.

2.2 What are Fractals?

Once it was believed that the geometry of nature centered on simple figures such as lines, circles, conic sections, polygons, spheres etc. Also, in the early days of mathematics and Euclidean geometry, objects have been classified as one-, two-, or three-dimensional (1D, 2D, or 3D). But many objects in nature are so complicated and irregular that we cannot use just the familiar objects from the classical Euclidean geometry to model them. For instance, how do we model mountains and trees in geometrical terms? Imagine the complexity of the network of paths that supply blood to and from every cell in the human body. Imagine also the intricate tree-like structures of lungs and kidneys [1], [2].

The term Fractal, which literally means broken or irregular fragments, was first coined by Benoit Mandelbrot in 1975, a pioneer in the field of fractal geometry, to describe a family of characteristic shapes that possess an inherent self-similarity in their geometric structure. He proposed that fractals and fractal geometry could be used to describe real objects that are difficult to define with Euclidean geometries, such as mountains, branching of trees, lightning and the density of clouds etc.

(a)

(b)

(c)

Figure 2.1: (a) fractal leaf (b) fractal lightning (c) fractal mountains

In most simple words, fractal can be defined as "a recursive object that has a fractional dimension showing shape similarity in scale".

2.3 Characteristic Features of Fractals

Almost all fractals have the following three characteristic features:

(1) Self-similarity
(2) Fractional dimension
(3) Infinite complexity and detail.

2.3.1 Self-similarity

In nature what is appealing to us is the repetition of patterns at all scales, no matter how small. A tree has branches. These branches have smaller branches, and so on. Theoretically the pattern branching is repeated infinitely many times, at ever-smaller scales. Similarly if we zoom in on a picture of a mountain, it will still look like a mountain. This is the characteristic self-similarity property of fractals.

In short, an object is self-similar only if you can break the object down into an arbitrary number of small pieces, and each of those pieces is a replica of the entire structure. Some examples of self-similarity are given in figure 2.2. The box indicates a few of the self-similarities of the object.

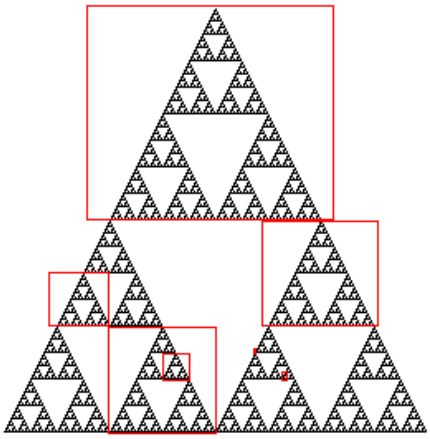

(a)

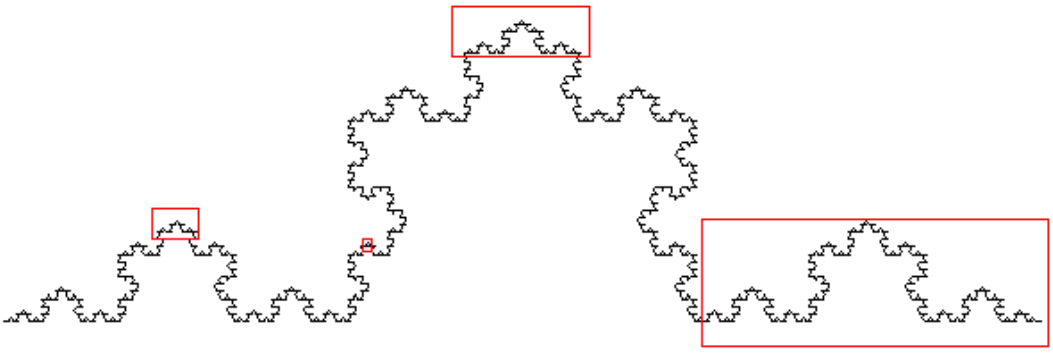

(b)

Figure 2.2: (a, b) Objects showing self-similarity

2.3.2 Fractional Dimension (Similarity dimension)

The second concept for a fractal is a fractional dimension. This concept distinguishes fractals from the Euclidean geometry, which have integer dimensions.

To explain the concept of fractal dimension, it is necessary to understand what we mean by dimension first. Obviously, a line has dimension 1, a plane dimension 2, and a cube dimension 3. But it is interesting if someone asks what the dimension of the Sierpinski triangle/ Koch curve is. Here comes the concept of fractal/self-similarity dimension.

We know that both the line and the square are self-similar. If a line segment is divided into 'N' equal pieces, each one being a scaled version of the original segment, with scaling factor 'r', the relation between 'N' and 'r' is

$$Nr = 1 \tag{2.1}$$

If a square is decomposed into 'N' self-similar copies, each one being a scaled version of the original square, with scaling factor 'r', then we have

$$Nr^2 = 1 \tag{2.2}$$

Similarly, if a cube has its sides scaled down by a factor 'r' into 'N' equal sub-cubes, then the relation is

$$Nr^3 = 1 \tag{2.3}$$

It is worth to note that the dimension of the object, whether it is one-dimensional segment, the two-dimensional square, or the three-dimensional cube, appears as the exponent of 'r' in the relation between 'N', the number of self-similar copies, and the scaling factor, 'r'. That is,

$$Nr^d = 1 \tag{2.4}$$

The interesting case occurs when the value of 'd' in the above equation is not an integer. When this happens, the object is said to be a self-similar fractal. The value of 'd' is called the fractal dimension or the similarity dimension.

The explicit formula for 'd' in terms of 'N' and 'r' can be written from equation 2.4 as

$$d = \frac{\log N}{\log\left(1/r\right)} \tag{2.5}$$

2.4 Fractal Classification

Generally speaking, fractal has two main geometric types. One is "random fractals" which are produced randomly from a set of non-determined steps, for example, most fractal objects found in nature. Another one is "deterministic fractals" which are produced as a result of an iterative algorithm (Iterated Function System, IFS) [1].
So, in the broadest sense, fractals can be divided into two categories:

- Objects that occur in Nature
- Mathematical constructions.

Natural objects exhibit scaling symmetry, but only over a limited range of scales. They also tend to be "roughly" self similar, appearing more or less the same at different scales of measurement. Sometimes this means that they are statistically self-similar; that is to say, they have a distribution of elements that is similar under magnification.

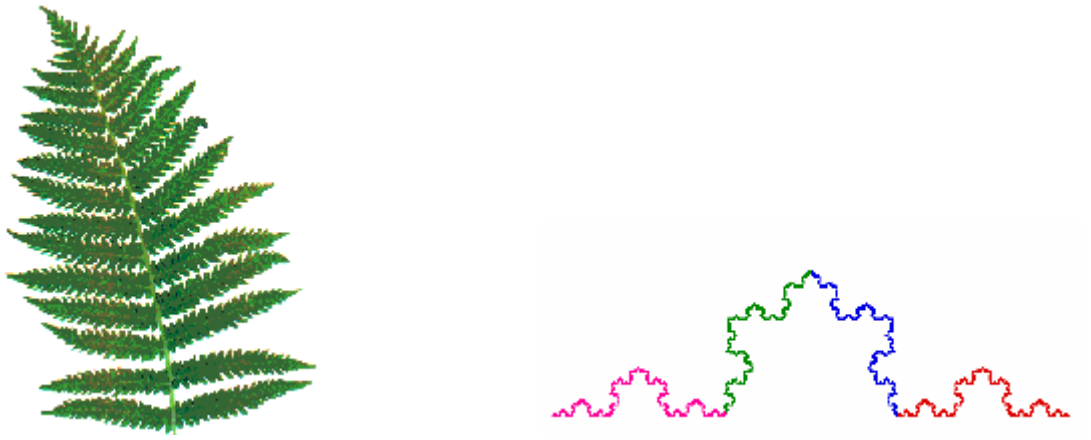

(a) (b)

Figure 2.3: Fractal Types (a) Fern (natural fractal) (b) Koch Curve (mathematical Construction)

In contrast to naturally occurring fractals, mathematical fractals can possess an infinite range of scaling symmetry. The more common constructions also tend to be exactly self-similar. Two simple examples are shown in figure 2.3.

2.5 Some Classical fractal Geometries (mathematical constructions)

2.5.1 Koch curve

Koch Curve, named after Helge Von Koch, is constructed with a straight line, by dividing it into three equal segments and replacing the middle segment by the two sides of an equilateral triangle of the same length as the segment being removed. Then taking each of the four resulting segments, divide them into three equal parts and replacing each of the middle segments by two sides of an equilateral triangle. This procedure is applied repeatedly to the remaining lines, as shown in figure 2.4.

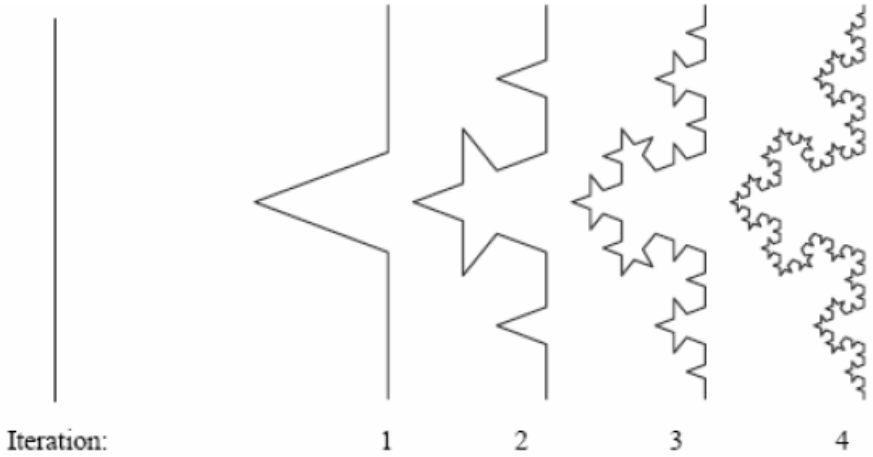

Figure 2.4: First four stages in the construction of Koch curve

In the limit there is a strictly similar structure as shown in figure 2.2(c). If this structure is scaled by a factor of r = 1/3, then there are N = 4 self-similar copies of the original one. Hence the fractional dimension'd', using equation 2.5, of Koch curve is

$$d = \frac{\log(4)}{\log(3)} \approx 1.2618$$

Another important property is that the Koch curve has infinite length. If the initial segment at stage 0 has length 1, then the curve at stage 1 has length 4/3. At the end of second stage, it has a length $4^2/3^2$. In the same way, the curve obtained after 'n' stages has length $4^n/3^n$. Therefore the limit curve has length

$$\lim_{n\to\infty} \frac{4^n}{3^n} = \infty$$

2.5.2 Sierpinski Gasket and Carpet

Sierpinski gasket is another good example of self-similar fractal, introduced in 1915 by the Polish mathematician W. Sierpinski.

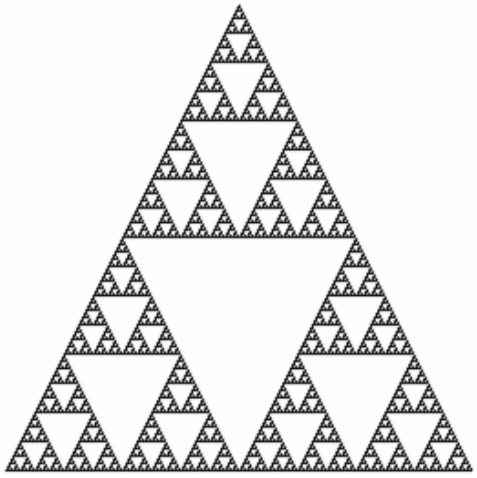

Figure 2.5: Ideal Sierpinski gasket

The deterministic construction algorithm for the Sierpinski gasket is shown in Figure 2.6. We begin with an equilateral triangle. Then use the midpoints of each side as the vertices of a new triangle, which is then removed from the original equilateral triangle. This process is continued; from each remaining triangle, we remove the middle one leaving behind three smaller triangles. This process is repeated infinitely many times.

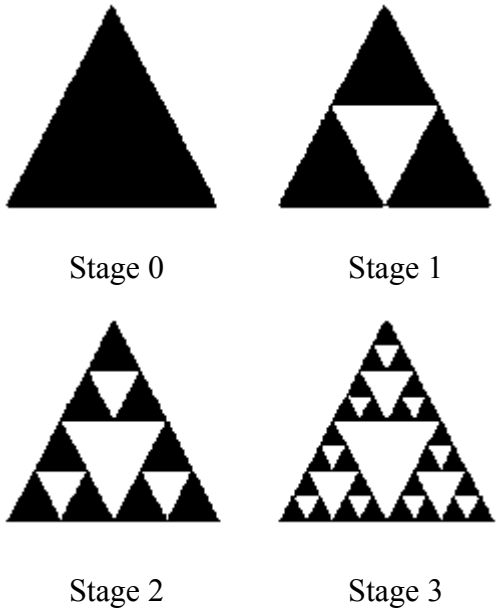

Figure 2.6: First three stages in the construction of Sierpinski gasket

From the construction, it is clear that the whole gasket is the union of N = 3 essentially disjoint scaled copies, where the scaling ratio is r = 1/2, so the fractal dimension is

$$d = \frac{\log(3)}{\log(2)} \approx 1.585$$

The Sierpinski carpet with its construction is shown in figure 2.7. It is a self-similar geometry with fractal dimension

$$d = \frac{\log(8)}{\log(3)} \approx 1.893$$

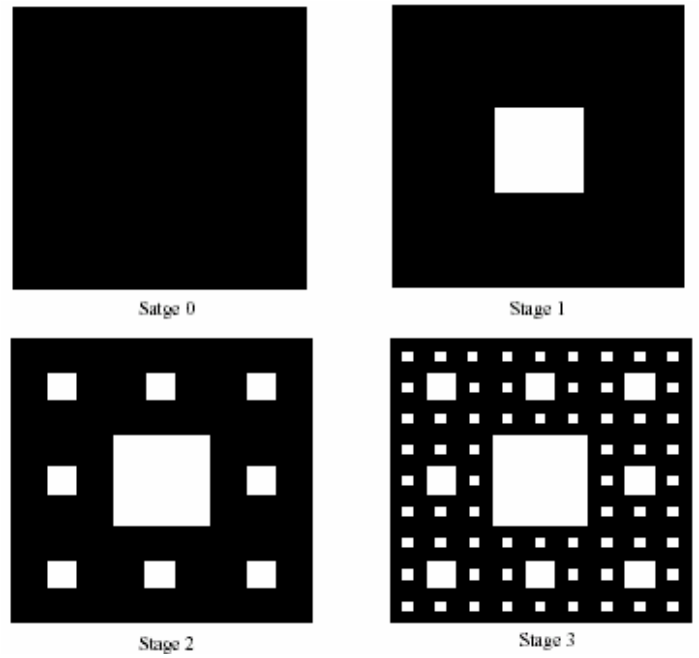

Figure 2.7: First three stages in the construction of Sierpinski Carpet

2.6 Iterated Function Systems

Iterated function system (IFS) is the mathematical language of fractals. It provides an extremely versatile tool for conveniently generating a wide variety of useful fractal structures. Iterated function system is based on a set of geometrical transformations called linear affine transformations w, which in turn is a composition of a linear transformation plus a translation, defined as

$$w\begin{pmatrix} x \\ y \end{pmatrix} = \begin{pmatrix} a & b \\ c & d \end{pmatrix}\begin{pmatrix} x \\ y \end{pmatrix} + \begin{pmatrix} e \\ f \end{pmatrix} \tag{2.6}$$

Or equivalently as

$$w(x, y) = (ax + by + e, cx + dy + f)$$

where a, b, c, d, e, and f are real numbers such that a, b, c, and d control rotation and scaling, while e and f control linear translation.

Now if $w_1, w_2, \ldots, w_N$ be a set of affine linear transformations and A be the initial geometry, then a new geometry can be formed by applying the set of transformations to the original geometry A and collecting together the results from $w_1(\mathrm{A}), w_2(\mathrm{A}), \ldots, w_N(\mathrm{A})$ in the following way:

$$W(A) = \bigcup_{n=1}^{N} w_n(A) \tag{2.7}$$

where W is known as the Hutchinson operator. A fractal geometry can be obtained by repeatedly applying W to the previous geometry in an iterative manner. For example, if the set A_0 represents the initial geometry, then this iterative process would yield a sequence of Hutchinson operators given by

$$A_1 = W(A_0), A_2 = W(A_1), \ldots, A_{k+1} = W(A_k)$$

An IFS generates a sequence that converges to a final image A_∞ in such a way that

$$W(A_\infty) = A_\infty$$

This image is called the attractor of the IFS and represents a "fixed point" of W, where the "points" in this case are actually defined as sets.

The IFS procedure for generating the well-known Koch fractal curve is demonstrated in Figure 2.8. In this case, the initial set A0 is the line interval of unit length. Four affine linear transformations (i.e., N = 4) are then applied to A0 as depicted in Figure 2.8. Next, the results of these four linear transformations are combined together using Eq. 2.7 to form the first iteration of the Koch curve, say A1. Applying the same four affine transformations to A1 and again using Eq. 2.7 to combine the results can then obtain the second iteration of the Koch curve. The first four iterations of the Koch curve are shown in Figure 2.9.

The IFS code for generating this object has also been provided in the figure 2.8.

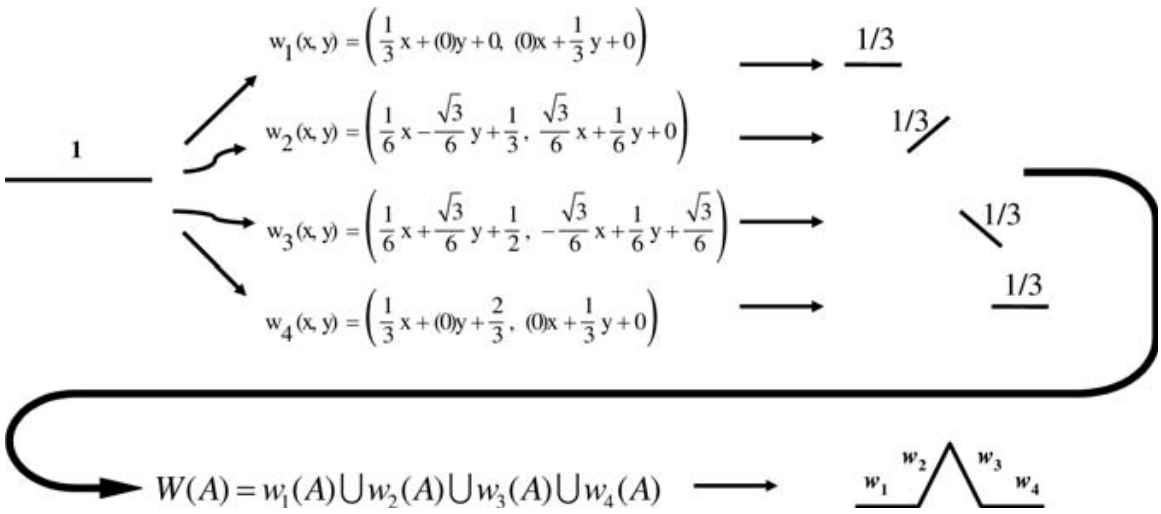

Figure 2.8: The standard Koch fractal curve as IFS

Figure 2.9: First four stages in the generation of Koch fractal curve via IFS approach

2.7 Fractal-Shaped antennas

Traditional approaches to the analysis and design of antenna systems have their foundation in Euclidean geometry. There has been a considerable amount of recent interest, however, in the possibility of developing new types of antennas that employ fractal rather than Euclidean geometric concepts in their design. Antennas based on fractal geometries are referred to as fractal-shaped antennas.

2.7.1 Key benefits of fractals in antenna design

As investigated and studied in [3]–[11], fractal geometries have revealed some well-known particular features in antenna design. We list down those key features as below.

Miniaturization: To be an efficient radiator an antenna's size must be appreciable portion of a wavelength. Therefore, antennas that operate at low frequencies are physically very large. This large size hinders their integration into smaller hand-held or man-wearable communication equipment. Fractals, due to their recursive nature and space filling properties, result in antennas that are electrically very long but fit into a compact physical area.

Multiple Resonances/wide band: For an antenna to be frequency-independent, it must be designed to have no characteristic size, or it must have many characteristic sizes to operate over many different frequency bands. Fractals have no characteristic size and due to self-similarity property, consists of multiple copies of themselves on various different scales, which enables them to result in frequency-independent or multifrequency antennas.

Efficiency and effectiveness: We know that radiation is produced because of time varying current or acceleration (or deceleration) of charge. Fractals are highly convoluted. Uneven shapes, sharp edges and sharp corners of fractals cause more abrupt changes in the current direction and hence result in enhanced radiation efficiently.
To conclude, the most interesting features of fractal-shaped antennas are miniaturization, wideband/ multiple resonances and high radiation efficiency.

2.7.2 Koch monopole antenna

The monopole antenna based on the Koch curve was studied in [4], [5] and it was shown that as compared to a straight wire monopole of the same height, the Koch monopole antenna has lower resonant frequency because the electrical size of the antenna increases as the number of iteration increases, as shown in figure 2.10 and hence it helps in antenna miniaturization.

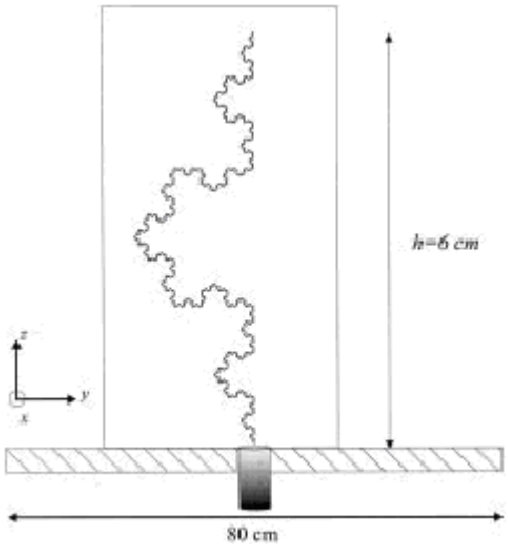

(a)

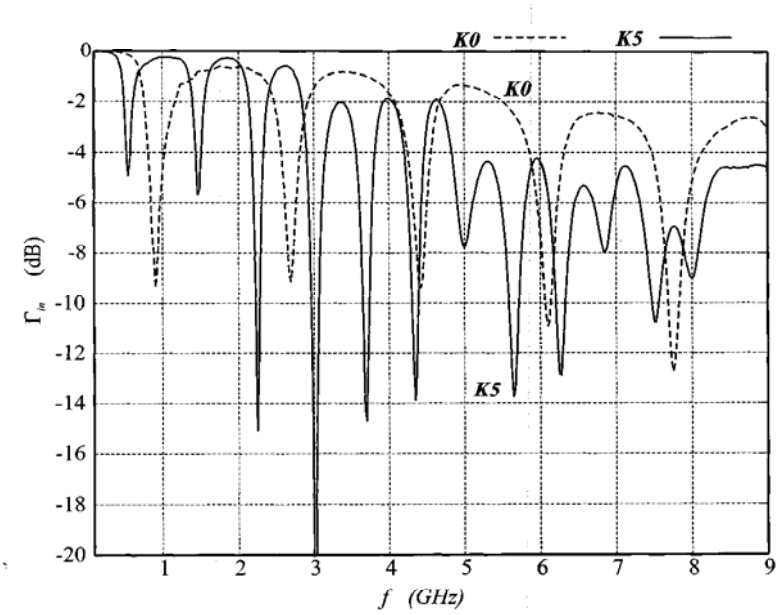

(b)

Figure 2.10: (a) Koch monopole antenna (b) Return Loss

In a large number of applications, and especially those involving mobile terminals, the reduction of the antenna size is an ultimate goal. The possibility to employ antennas that fit in smaller volumes, but still with an efficient behavior, is certainly appealing.

2.7.3 Fractal loop antennas

Loop antennas [6] are well understood and have been studied using a variety of Euclidean geometry. The have distinct limitations, however. Resonant loop antennas require a large amount of space and small loops have very low input resistance. A fractal island can be used as a loop antenna to overcome these drawbacks. Two possible fractals fed as loop antennas [7] are depicted in Figure 2.11.

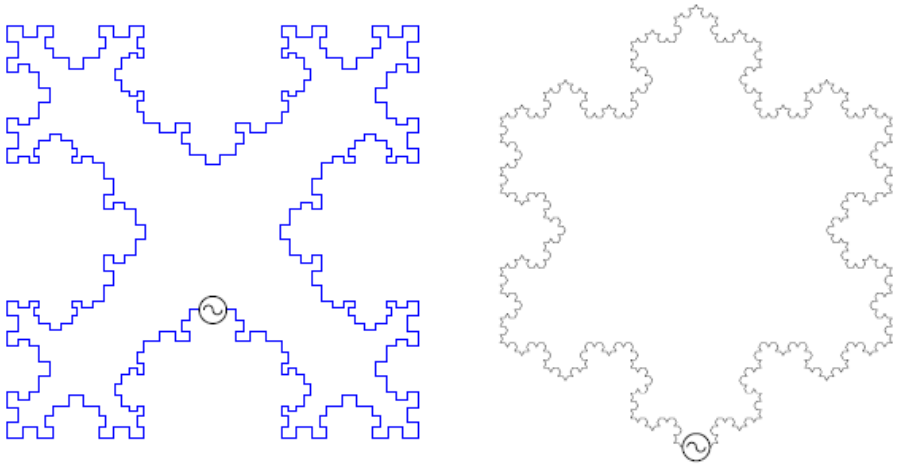

(a) (b)

Figure 2.11: Two fractal loop antennas (a) Koch loop (b) Minkowski loop

Fractals loops have the characteristic that the perimeter increases to infinity while maintaining the volume occupied. This increase in length decreases the required volume occupied for the antenna at resonance. For a small loop, this increase in length improves the input resistance. By raising the input resistance, the antenna can be more easily matched to a feeding transmission line.

A comparison of the input resistance variation with respect to the electrical perimeter of a Circular loop and a Koch loop is given in Figure 2.12.

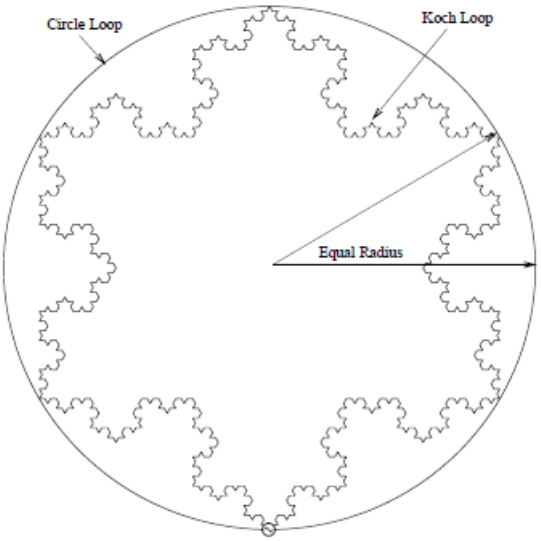

(a)

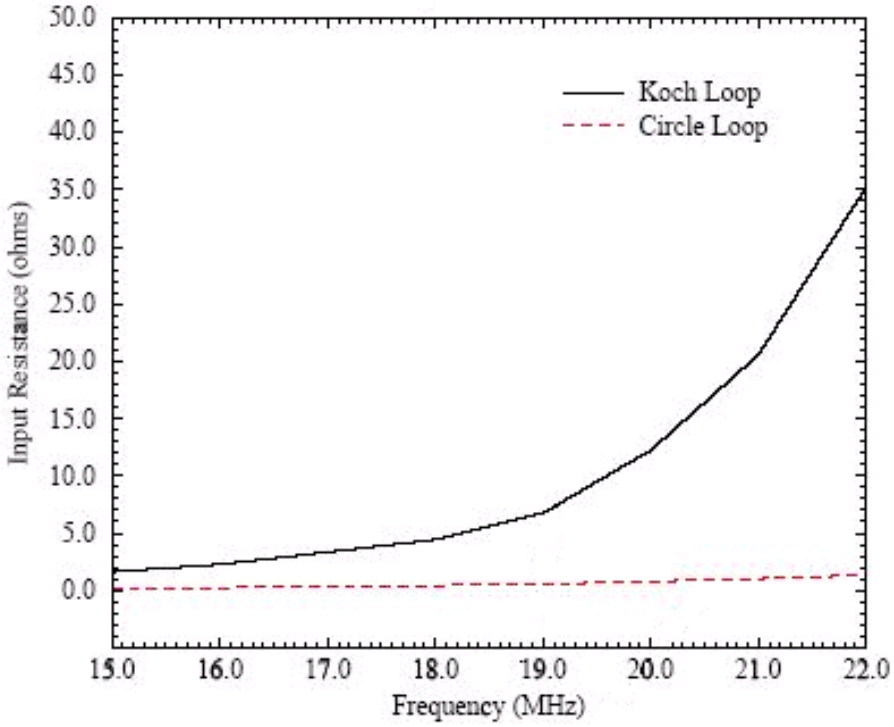

(b)

Figure 2.12: (a) Circular loop vs. Koch loop of equal volume (b) input resistance with regarding to perimeter

It is clear that the input resistance of the fractal loop increases at a much higher rate that the circular loop.

2.7.4 Sierpinski Carpet Patch Antenna

A microstrip antenna based on the Sierpinski carpet fractal geometry was designed and analyzed in [8], [9]. The fabricated antenna with its return loss is shown in figure 2.13.

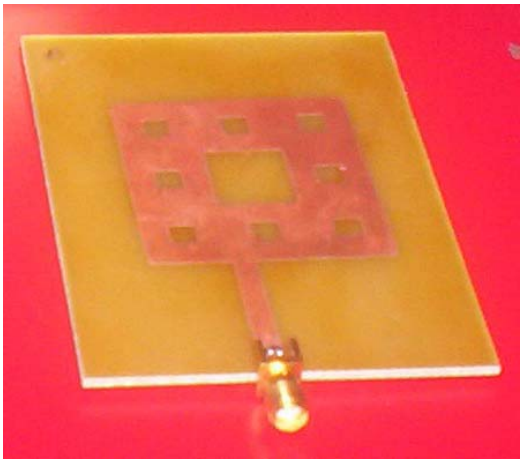

(a)

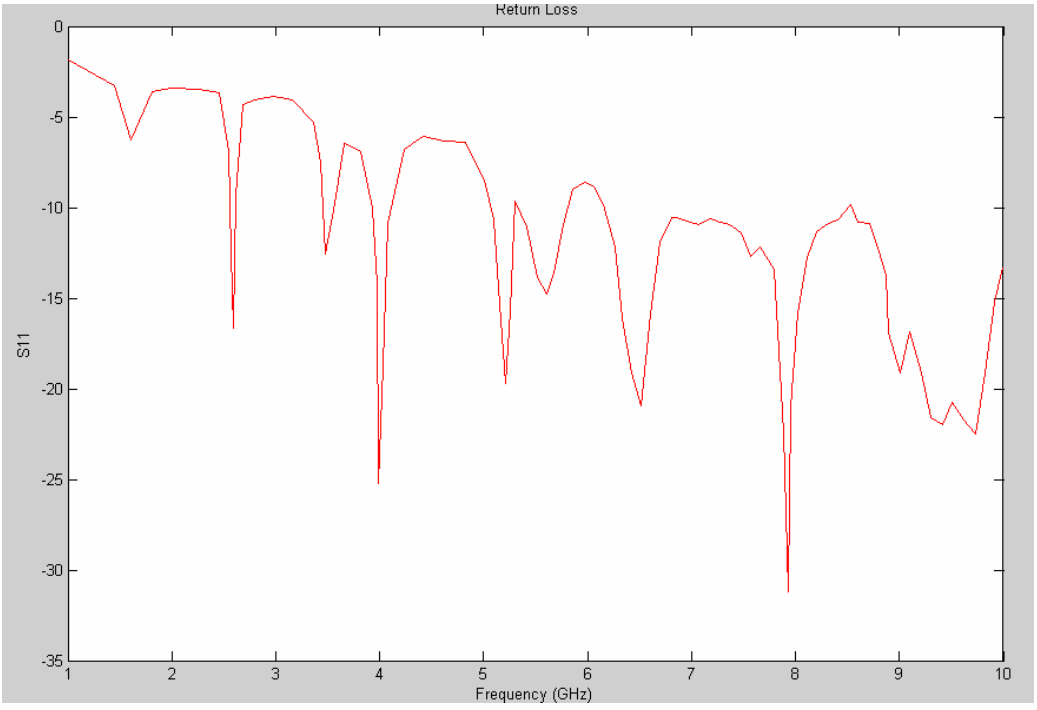

(b)

Figure 2.13: (a) Sierpinski Carpet Patch Antenna (SCPA) (b) Return loss of SCPA

It was shown that the Sierpinski carpet patch antenna could provide a multiband operation. The basic square patch antenna operates at one frequency only but as the

number of iterations is increased in the Sierpinski carpet fractal, the number of resonant frequencies is also increased. This is due to the self-similarity properties of the fractal structure.

2.7.5 Fractal multiband antenna based on the Sierpinski gasket

Carles Puente for the first time employed the self-similar nature of fractals for the development of multiband antennas [10]. He designed a monopole antenna based on the Sierpinski fractal geometry as shown in the figure 2.14. The fractal shape was constructed through five iterations.

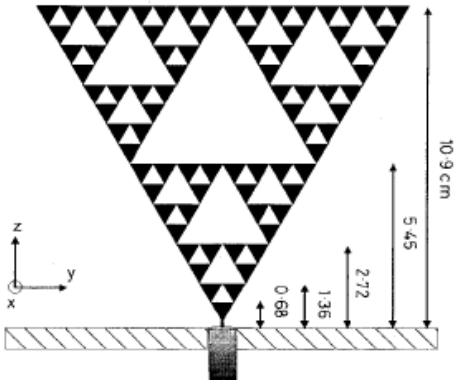

Figure 2.14: Original Sierpinski monopole antenna by Puente

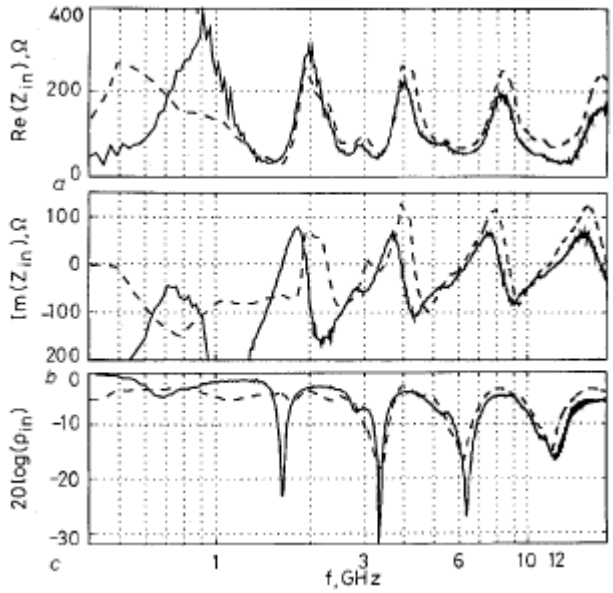

Figure 2.15: Original Sierpinski monopole (a) Input resistance (b) Input reactance (c) Input return loss

Experimental results, as shown in figure 2.15, displayed a multi-band behavior through the five bands. Dr. Puente came to the conclusion that the bands show a notable degree of similarity and also the bands are spaced by a log-period of 2, the same factor that relates the geometrical self-similarity. Hence it was concluded that the geometrical self-similarity of the fractal structure is translated into its electromagnetic behavior.

CHAPTER 3. DESIGN OF THE SIERPINSKI GASKET MONOPOLE ANTENNA

3.1 Introduction

This chapter deals with the design of the Sierpinski gasket monopole antenna (SGMA). The aim of building this monopole is to design a single element antenna that can operate at multiple frequencies. The generation of the Sierpinski geometry is first described. In the next section, the antenna description and the simulated results are given. Finally a comparison of the Sierpinski monopole with triangular monopole antennas is discussed.

3.2 Generation of Sierpinski Fractal Geometry

Two approaches can be used for the generation of Sierpinski fractal geometry.

1. Decomposition Approach
2. Iterated function system

3.2.1 Decomposition Approach

The procedure for geometrically constructing this fractal begins with an equilateral triangle contained in the plane, as illustrated in Stage 0 of Figure 3.1. The next step in the construction process (see Stage 1 of Figure 3.1) is to remove the central triangle with vertices that are located at the midpoints of the sides of the original triangle, shown in Stage 0.This process divides the original triangle to three scaled down (half sized) versions of the larger triangle. This process is then repeated for the three remaining triangles, as illustrated in Stage2 of Figure 3.1.

The Sierpinski-gasket fractal is generated by carrying out this iterative process an infinite number of times. It is clear from its generation that the Sierpinski gasket is an example of self-similar fractal.

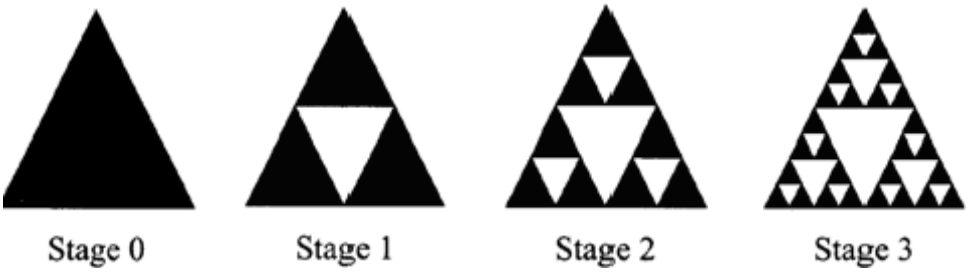

Figure 3.1: Decomposition approach

3.2.2 Iterated function System Approach

It is assumed that the origin of the coordinate system is at the bottom left corner of the larger triangle and the x-axis pass through the base (bottom) side of the triangle. The transformations w_1, w_2, w_3 are indicated in the figure 3.2.

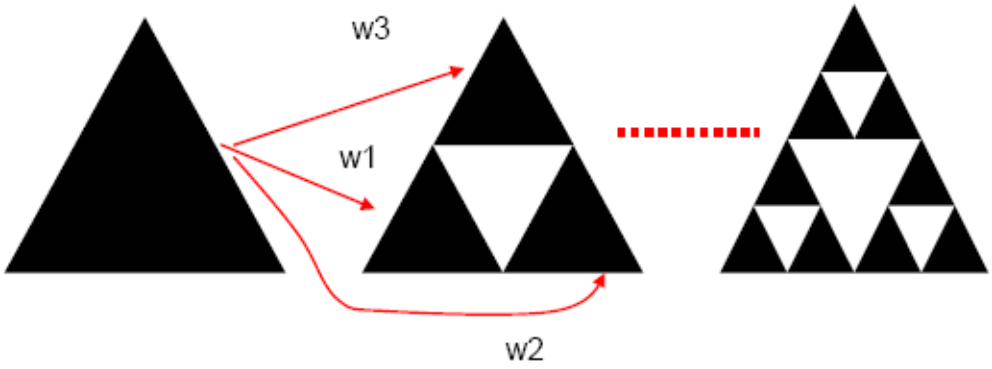

Figure 3.2: IFS for generation of Sierpinski Fractal Geometry

$$\left.\begin{aligned} w_1\begin{pmatrix} x \\ y \end{pmatrix} &= \begin{pmatrix} 0.5 & 0 \\ 0 & 0.5 \end{pmatrix}\begin{pmatrix} x \\ y \end{pmatrix} + \begin{pmatrix} 0 \\ 0 \end{pmatrix} \\ w_2\begin{pmatrix} x \\ y \end{pmatrix} &= \begin{pmatrix} 0.5 & 0 \\ 0 & 0.5 \end{pmatrix}\begin{pmatrix} x \\ y \end{pmatrix} + \begin{pmatrix} 0.5 \\ 0 \end{pmatrix} \\ w_3\begin{pmatrix} x \\ y \end{pmatrix} &= \begin{pmatrix} 0.5 & 0 \\ 0 & 0.5 \end{pmatrix}\begin{pmatrix} x \\ y \end{pmatrix} + \begin{pmatrix} 0.25 \\ 0.433 \end{pmatrix} \end{aligned}\right\} \quad (3.1)$$

$$W(A) = w_1(A) + w_2(A) + w_3(A) \quad (3.2)$$

The same process is carried out on the three half sized triangle obtained and so on after infinite number of iterations the ideal Sierpinski gasket is obtained.

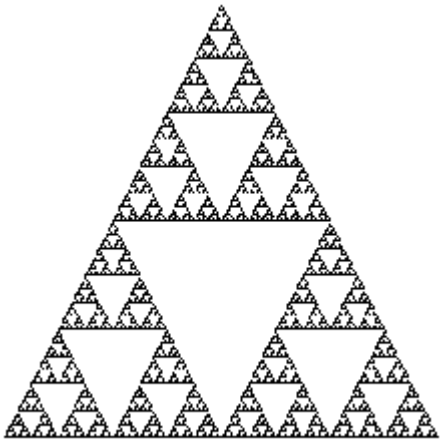

Figure 3.3: Ideal Sierpinski Gasket

In such an ideal structure, each one of its three main parts is exactly equal to the whole three gaskets but scaled by a factor of two and so are each of the three gaskets that compose any of those parts.

3.3 Antenna Description

A monopole antenna based on the Sierpinski gasket constructed through three iterations with a scale factor of 2 and with a flare angle of 60 degrees is shown in Figure 3.4.

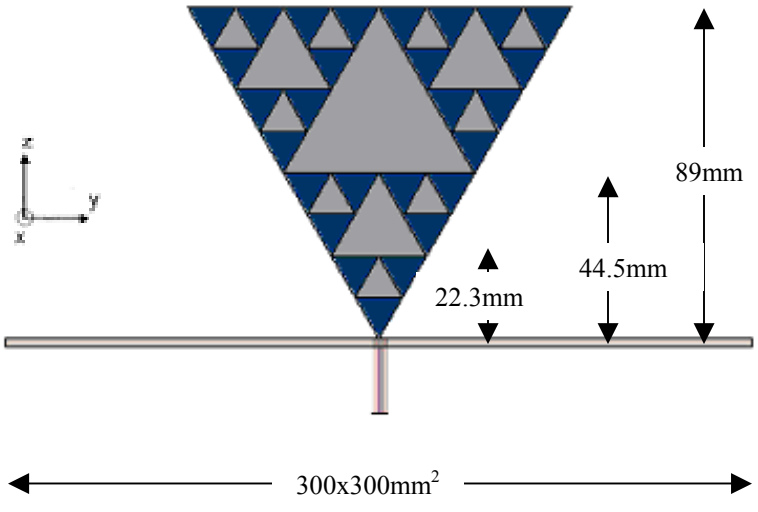

Figure 3.4: Sierpinski Monopole Antenna

The height of the Sierpinski fractal is chosen as 89mm based on the fractal used in the literature [11] and the empirical relation

$$f_n \approx (0.17 + 0.44n)\frac{c}{h} \tag{3.3}$$

from Brown and Woodward [12].

The Sierpinski gasket was chosen as the first candidate for a fractal antenna due to its resemblance to the triangular antenna. As shown in the figure, the Sierpinski triangle is printed on a 1 mm thick FR4 substrate ($\varepsilon_r = 4.4$) and mounted over a 300 x 300 mm^2 ground plane. The antenna is fed through the underside of the ground plane by a 50 Ohm coaxial probe.

The gasket has been constructed through three iterations here, so three scaled versions of the Sierpinski gasket are found on the antenna as shown in the figure 3.4. If we neglect the contribution of the center holes to the antenna performance and consider the fact that the current flowing from the feeder should concentrate over a region that is comparable in size to the wavelength, a behavior similar to three scaled bow-tie monopole antennas with heights equal to those of sub-gaskets could be expected. In other words, keeping in mind the self-similarity property, we can assume that electromagnetic waves while traveling from the apex to the to flat end will become radiated by sub-gaskets when the wave finds a gasket comparable in size to its wavelength.

The scale factor among the three sub-gaskets is $\delta = 2$, where

$$\delta = \frac{h_n}{h_{n+1}} \tag{3.4}$$

where ‘h’ represents the height of the gaskets and ‘n’ is a natural number, therefore, one should look for similarities at frequencies also spaced by a factor of two.

Note that $h_1 = h$ is the height of the largest gasket.

3.4 Simulation of Sierpinski Monopole Antenna using Ansoft HFSS

The construction and simulation of the 3rd iterated Sierpinski monopole antenna is carried out using FEM based electromagnetic simulator, Ansoft HFSS.

The schematic of the Sierpinski monopole antenna in HFSS is shown in figure 3.5.

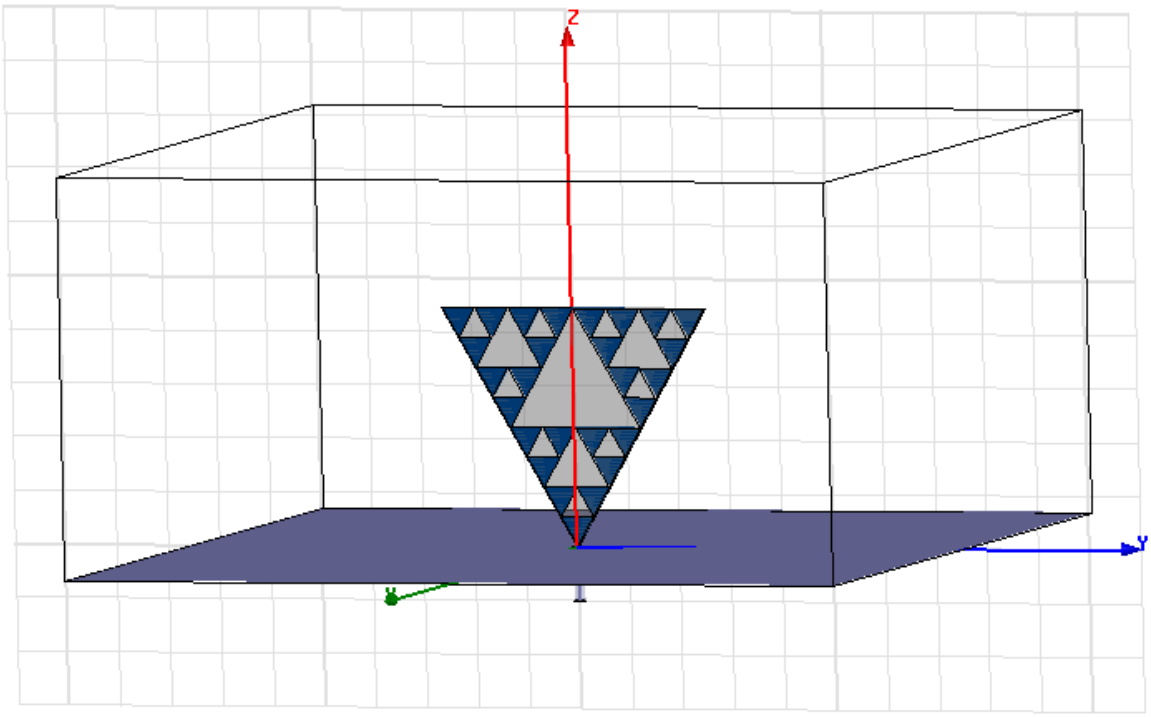

Figure 3.5: Schematic of Sierpinski Monopole Antenna in Ansoft HFSS

A wave port was used to excite the Sierpinski monopole antenna. An integration line was defined to specify the direction of the excitation field pattern and to compute the Zpv or Zvi impedance for the port. The coaxial line was modeled in HFSS by drawing two concentric cylinders. The outer cylinder was filled with Teflon and the inner cylinder was modeled as a perfect electric conductor. The bottom ground plane, top-radiating antenna was modeled as sheet conductor and finite conductivity boundary was assigned to each of them to include the copper loss. An air box was used around the monopole antenna to create virtual object representing the radiation boundary. A radiation boundary was then assigned to the air box. The virtual air box was placed such that it was located lambda/4 from the radiating antenna from all four sides.

3.4.1 Input Impedance and Return Loss

The simulated results for magnitude of the input reflection coefficient relative to 50 ohm and the input impedance, both real and imaginary parts, are shown in the figures 3.6, 3.7 respectively.

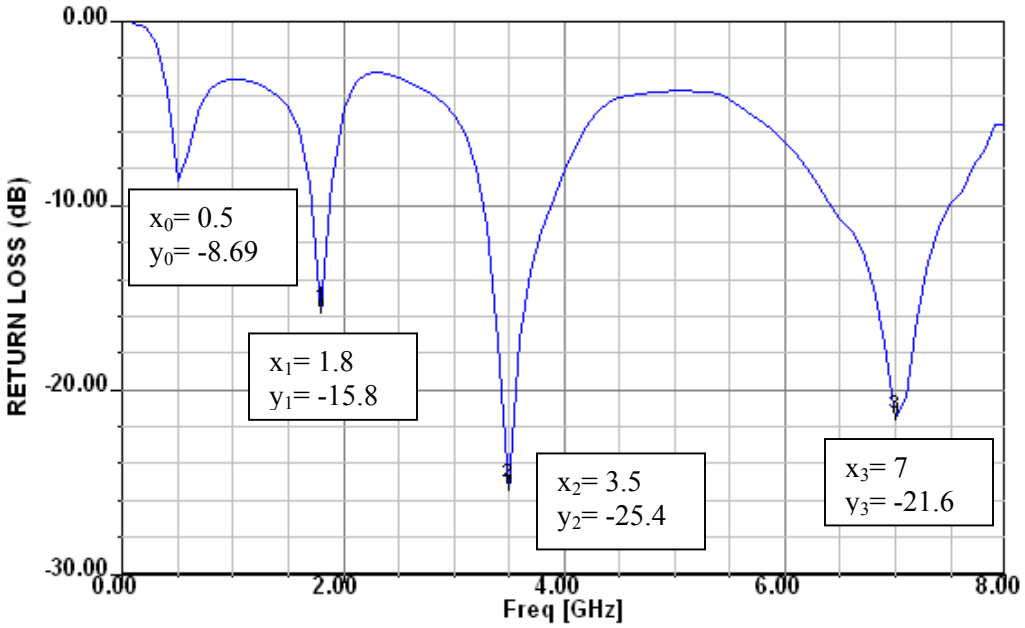

Figure 3.6: Simulated Return Loss of Sierpinski Monopole Antenna in Ansoft HFSS

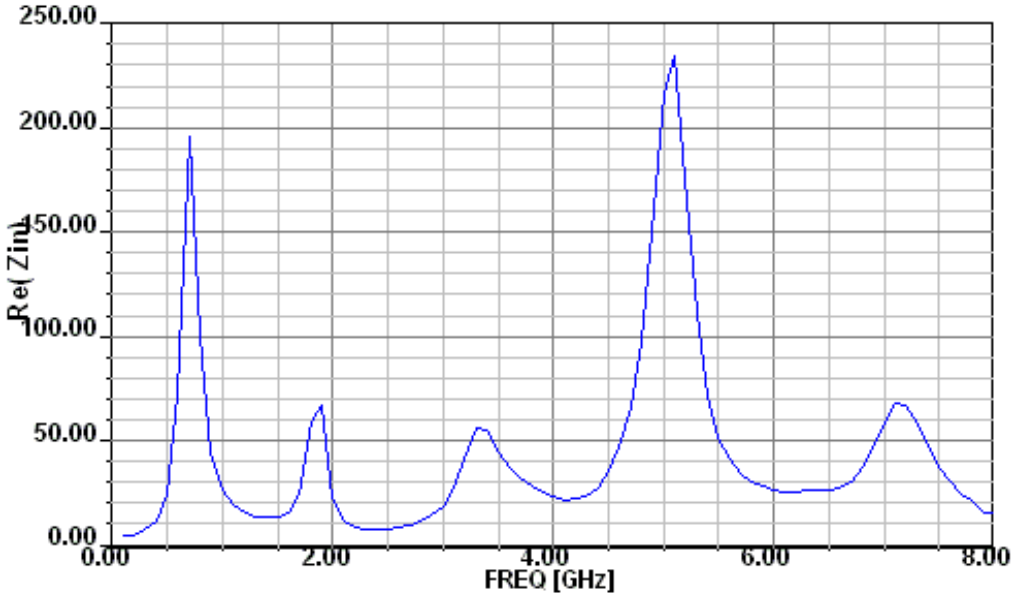

(a)

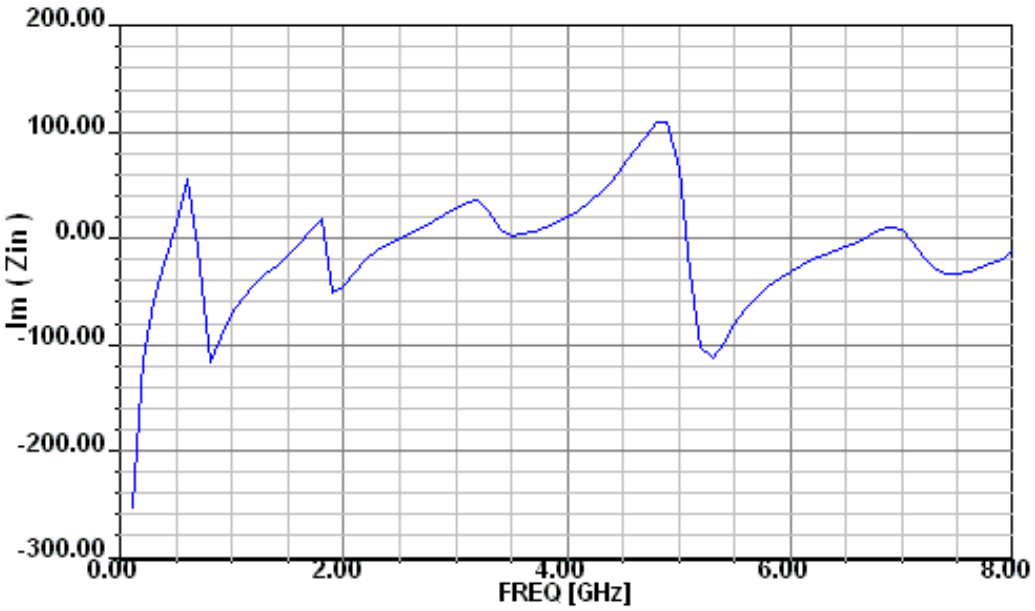

(b)

Figure 3.7: Simulated Input Impedance in Ansoft HFSS (a) Real part (b) Imaginary part

These plots are a clear manifestation of the multi-band behavior of the Sierpinski monopole antenna. Each of these three plots shows three log-periodically spaced bands. The Sierpinski monopole is well matched (VSWR<2) at the three upper bands at which the input resistance approaches 50 Ohm and the input reactance approaches zero.

The main features derived from this plot are given in the table 3.1.

n (Band)	f_n (GHz)	BW (%)	L_r (dB)	f_{n+1}/f_n	h_n/λ_n
0	0.5	-	-8.71	3.6	0.15
1	1.8	9	-14.8	1.94	$0.53 \approx 0.26\,\delta$
2	3.5	18	-24.25	2	$0.52 \approx 0.26\,\delta$
3	7	14	-18.61	-	$0.52 \approx 0.26\,\delta$

Table 3.1: Main Parameters of the simulated Sierpinski Monopole

The four bands shown in the 1st column of the table are picked at the four lowest input return loss points. The frequencies corresponding to such minimums appear in the 2nd column. The third column represents the relative bandwidth of each band for Return Loss < -10. The fourth column represents the input return loss, the fifth one describes the frequency ratio between adjacent bands and the sixth one the ratio between the height of the each of the sub-gaskets and the corresponding band frequency.

It is clear from the table that the three upper bands are log-periodically spaced by a factor of 2, which is the same scale factor that characterizes the Sierpinski fractal geometry. This shows that self-similarity in the geometry is translated into the electromagnetic behavior. The Sierpinski fractal geometry considered here is a third iteration Sierpinski fractal geometry and the number of log-periodic bands are also three, so we can say that number of log-periodic bands are proportional to the number of fractal iterations. Hence we can control the number of operating log-periodic frequency bands with the number of iterations, which is a great advantage of the Sierpinski Fractal Multi-band Antenna as compared to other conventional multi-band antennas.

This table suggests that the antenna is matched approximately at frequencies

$$f_n \approx 0.26 \frac{c}{h} \delta^n \tag{3.5}$$

where c is the speed of light in vacuum, h is the height of the largest gasket, δ is the log period ($\delta = 2$) and n a natural number.

Looking at the first band, it is important to notice that log-periodic behavior is lost in the lower band. This fact can be related to the antenna truncation effect since the structure is not an ideal fractal constructed after an infinite number of iterations. In other words, the largest triangle lacks of larger fractal iterations breaking this way the symmetry with respect to the central bands. Although an ideal fractal shape is self similar [1] at an infinite number of scales, a practical implementation of the structure requires it to be of finite iteration.

3.4.2 Radiation Patterns

To consider an antenna as a multi-band, the input impedance as well as the radiations patterns within the different resonances must be similar. Since, here the whole frequency range is very large, strict agreement among the patterns cannot be assumed.

The simulated results for the 2-D radiation patterns are shown in the figure 3.8. The main cuts of the total E-field component for the elevation plane (ϕ=0° and ϕ=90°) and azimuth plane (θ=90°) are simulated at the three log-periodic bands, each cut is taken at the return loss minimum of the corresponding band. Also the cuts are normalized with respect to the absolute pattern maximum.

The radiation patterns given in figures above demonstrate that the main features of the radiation patterns are almost kept similar through the bands with a two-lobe structure. Also, the antenna has a tendency to enhance radiation in the x-direction, which is obvious from the geometry of the antenna, since the antenna is planar and has a larger extension in the yz-plane.

There are some disagreements among the patterns also. The lobe closest to the zenith shows a larger ripple content at higher frequencies. This behavior can be linked to the non-multiband performance of the finite ground plane; the currents flowing over it can become reflected at edges of the ground plane resulting in a standing wave distribution which would have the most important contribution to the radiation along the plane's orthogonal direction. And it is due to this reason that the expected null in the z-direction is hidden. Since the square ground plane is not self-scalable, its size relative to

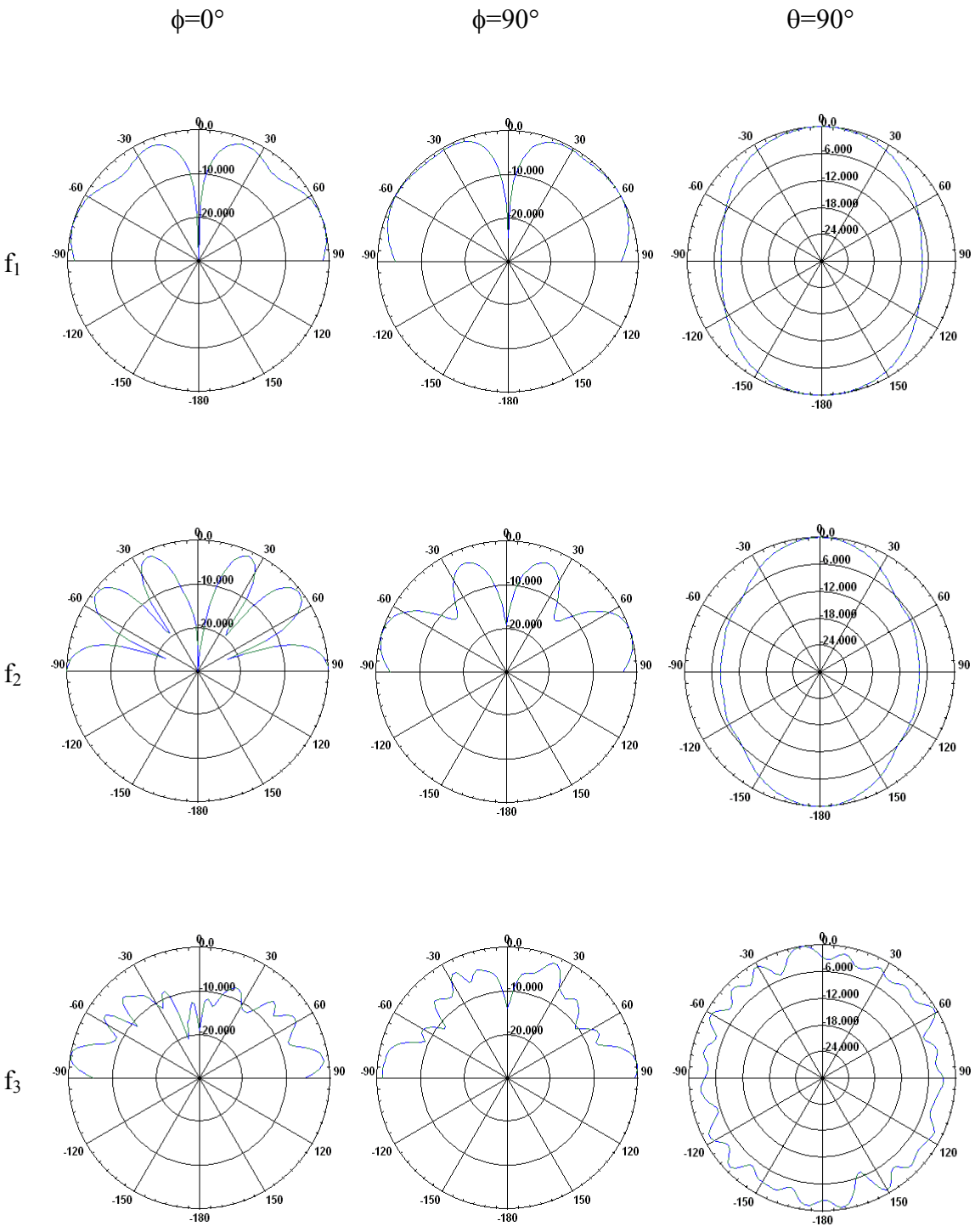

Figure 3.8: Simulated Radiation Patterns of Sierpinski Monopole Antenna in Ansoft HFSS

wavelength is larger at the upper bands resulting in an interference pattern with faster variations, which might explain the pattern ripple at the upper bands.

The effect of the finite size of the ground plane must be taken into account when analyzing the patterns. For instance, those at the upper bands show a characteristic ripple, which is due to diffraction at the edges of the ground plane. The variations on the ripple are faster when frequency is increased since the squared plane is obviously not self-scalable and the edges are spaced a longer distance in terms of the corresponding wavelength.

The simulated gain of the antenna at the three log-periodic frequencies is given in table 3.2.

Band	Gain (dBi)
I	5
II	7
III	10

Table 3.2: Simulated Gain of Sierpinski Monopole Antenna

3.5 Simulation of Sierpinski Monopole using Microwave Studio of CST

The Sierpinski monopole antenna is also simulated using a 3-D finite integration time domain (FITD) software package, Microwave Studio of CST.

The schematic of Sierpinski monopole antenna in Microwave Studio of CST is given in figure 3.9

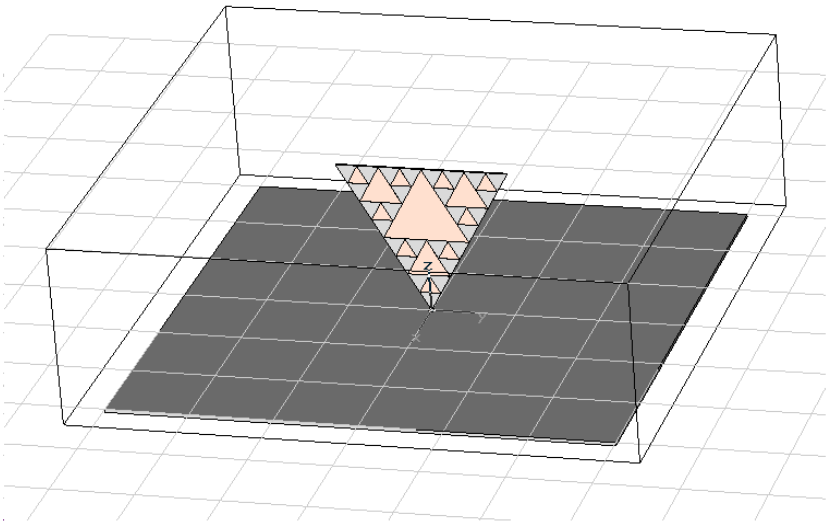

Figure 3.9: Schematic of Sierpinski monopole antenna in Microwave Studio of CST

3.5.1 Simulated Results of Sierpinski Monopole Antenna

The simulated return loss and radiation patterns of the Sierpinski monopole antenna using Microwave Studio (MWS) of CST are given in figure 3.10 and 3.11 respectively. All these results are in good agreement with those obtained using Ansoft HFSS.

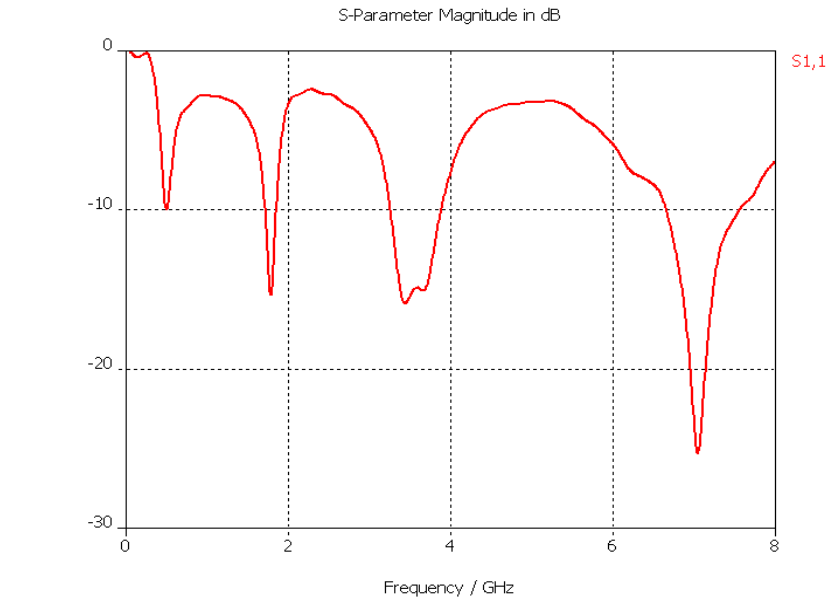

Figure 3.10: Simulated Return Loss of Sierpinski Monopole Antenna in MWS of CST

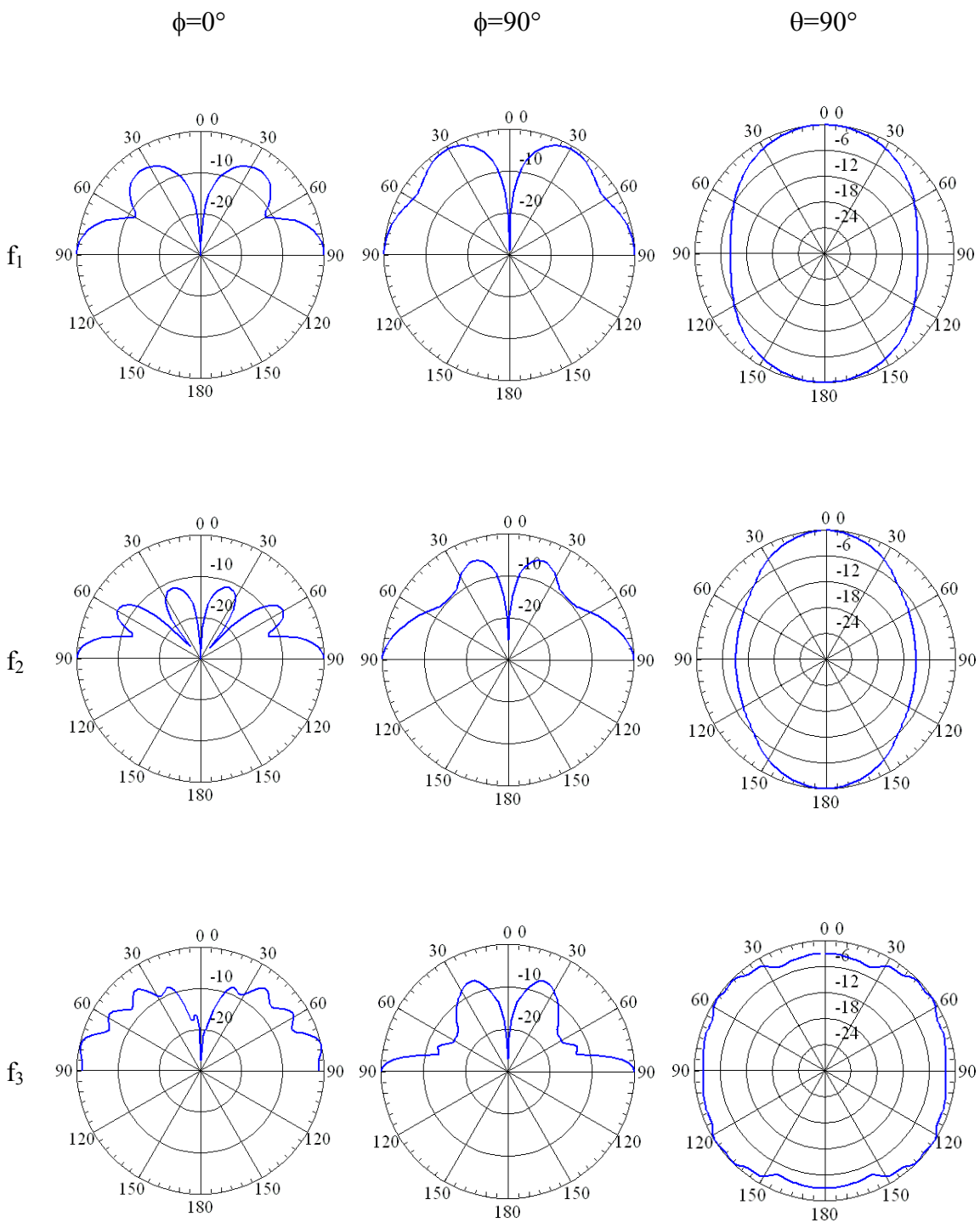

Figure 3.11: Simulated Radiation Patterns of Sierpinski Monopole Antenna in MWS of CST

3.6 Comparison of Simulations with Ansoft HFSS and MWS of CST

The Sierpinski Monopole Antenna was 1st simulated in FEM based electromagnetic simulator, Ansoft HFSS. The frequency sweep for the Sierpinski Monopole Antenna is very large, from 100 MHz to 8 GHz, hence the simulation in Ansoft HFSS took very long time for completion and the memory requirements are also very large. Then the simulation of the antenna was performed in FITD based electromagnetic simulator, MWS of CST. This simulator took very less time as compared to Ansoft HFSS for completion of simulation and also the memory requirements are low.

The results obtained from simulating the Sierpinski Monopole Antenna in Ansoft, HFSS and MWS of CST are similar to each other as shown in figure 3.12 and 3.13. Figure 3.12 shows that the resonant frequencies appear at the same position in both the cases. There is slight difference in the return loss at the resonant frequencies for the two cases, which can be attributed to the fact that in Ansoft HFSS, the radiation boundary (Air box size) is

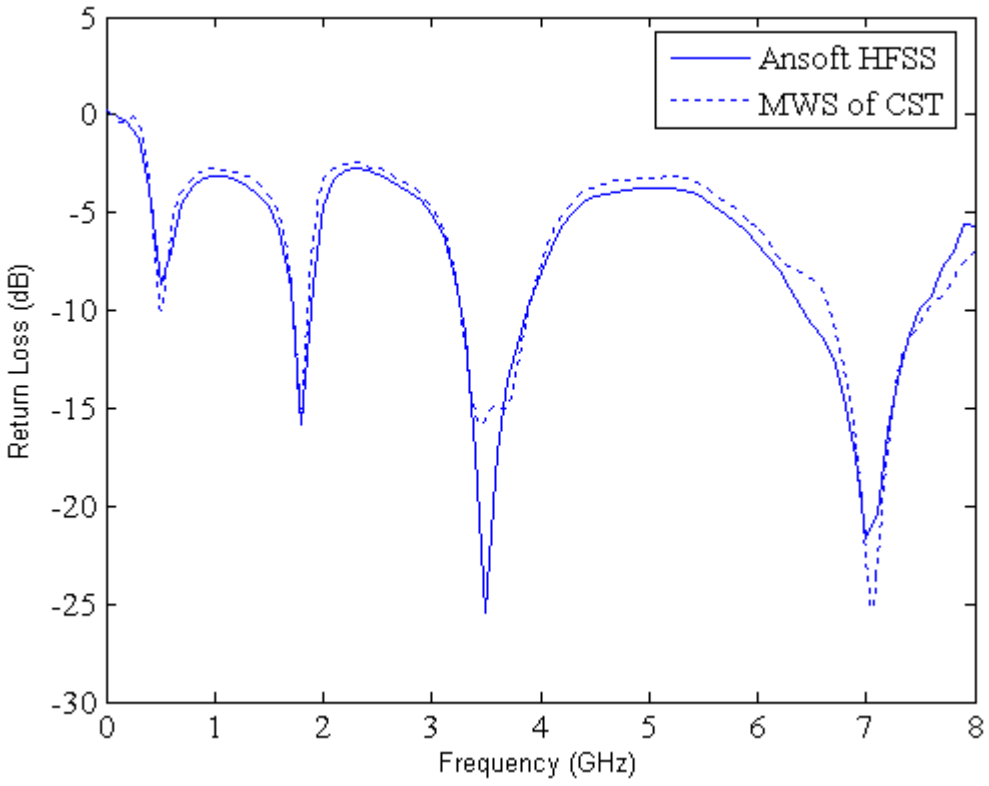

Figure 3.12: Return Loss of Sierpinski monopole antenna in HFSS and CST

defined by the user whereas in MWS of CST there is an option that automatically defines the Air Box size at the center frequency of the sweep.

The solid line in figure 3.13 shows the radiation patterns obtained from simulation in MWS of CST where as the dotted line shows those obtained from Ansoft HFSS. Clearly, the main features of the patterns obtained from the two simulators are almost similar with slight variations. So it is advisable to use MWS of CST for simulating such broadband structure.

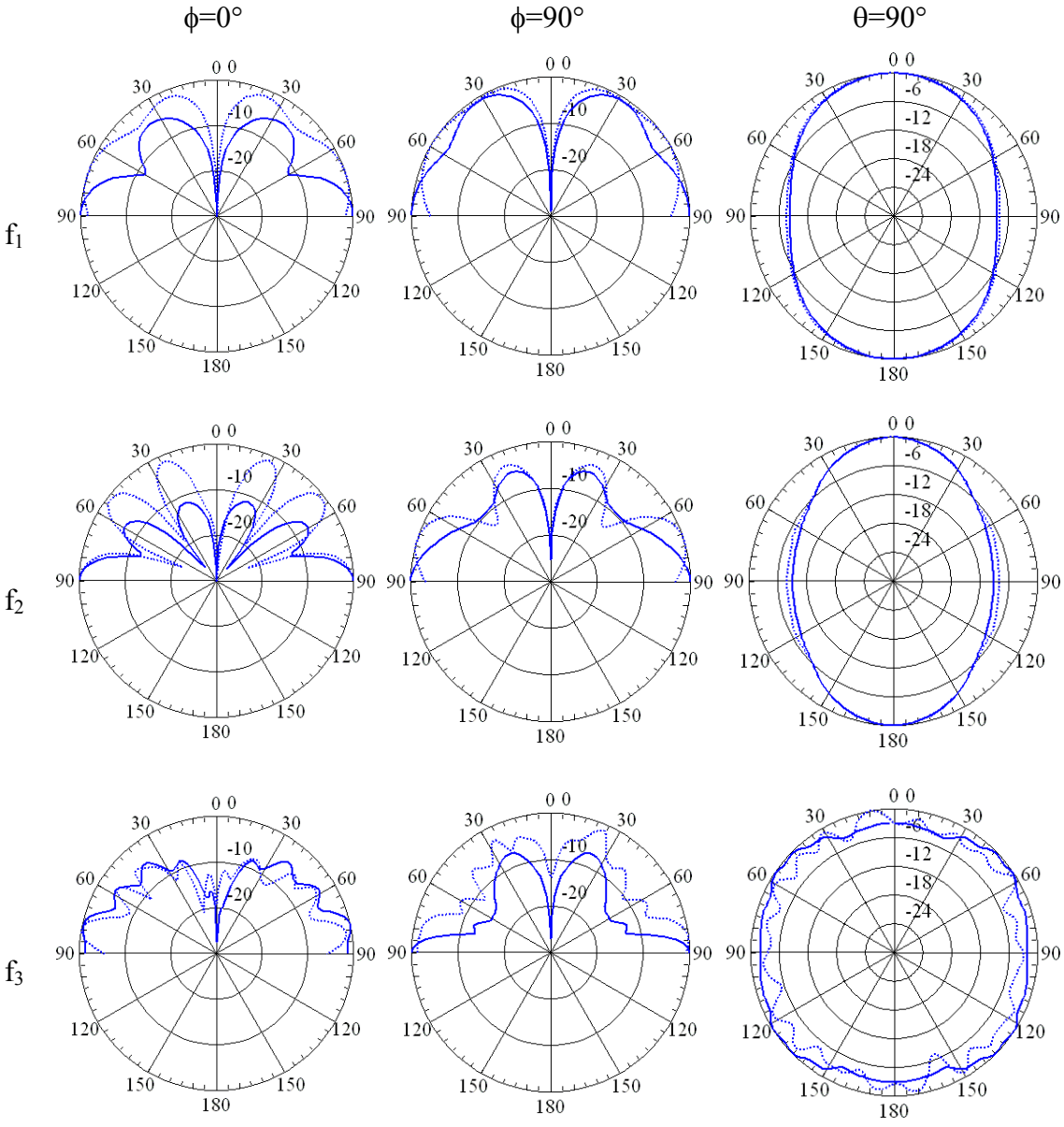

Figure 3.13: Radiation Patterns of Sierpinski monopole antenna in HFSS and CST

3.7 Comparison with the Triangular Monopole Antenna

The Sierpinski monopole antenna is similar to the Euclidean triangular monopole antenna. A detailed analysis of the triangular monopole antennas was performed in [12]. Since the Sierpinski geometry considered here is generated after three iterations, three self-similar sub-gaskets appear on the Sierpinski geometry as shown in the figure 3.4. Now to get more insight on the behavior of the Sierpinski monopole antenna, three triangular monopole antennas as shown in figure 3.14, each of the size of the three sub-gaskets, are simulated using Ansoft HFSS.

Figure 3.15 shows the input reflection coefficient relative to 50Ω of the three-monopole bow ties together with the Sierpinski monopole (the plot corresponding to the Sierpinski antenna appears at the bottom of the figure).

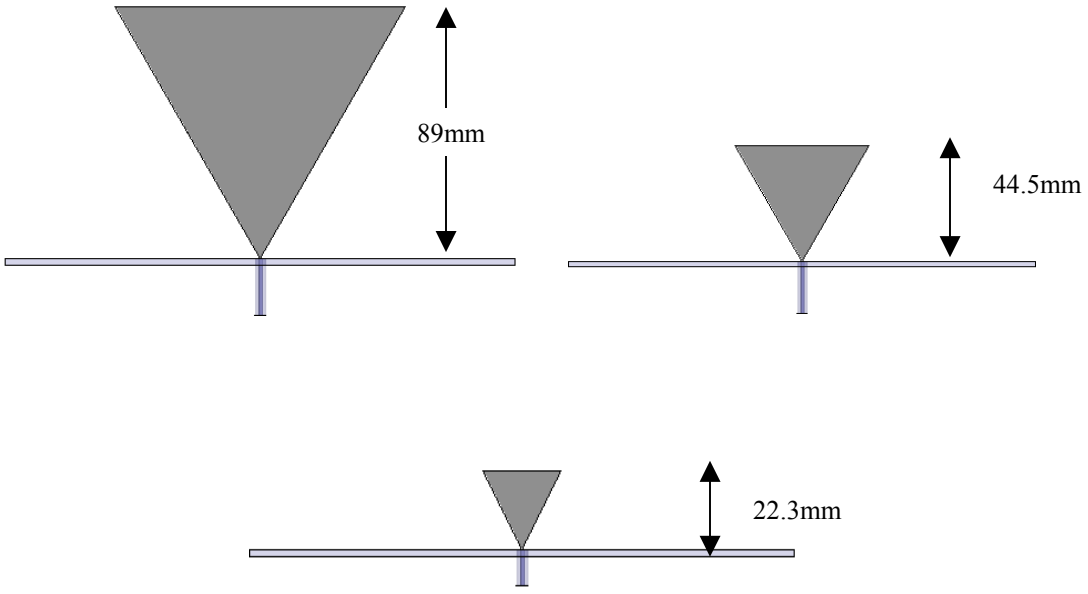

Figure 3.14: Triangular monopole antennas

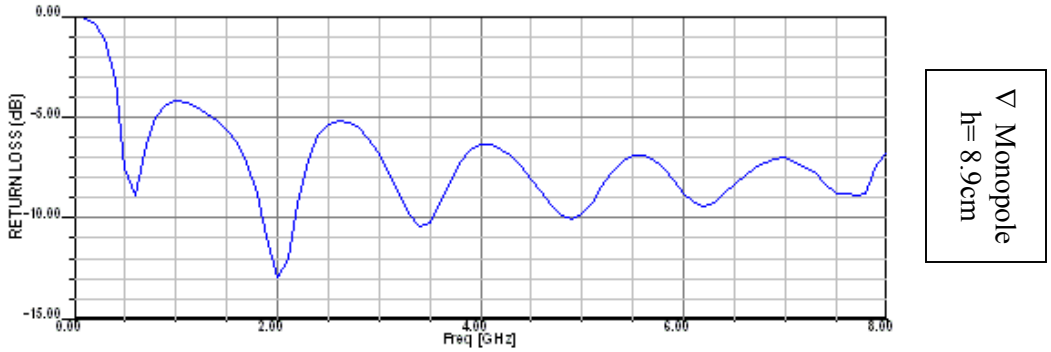

(a)

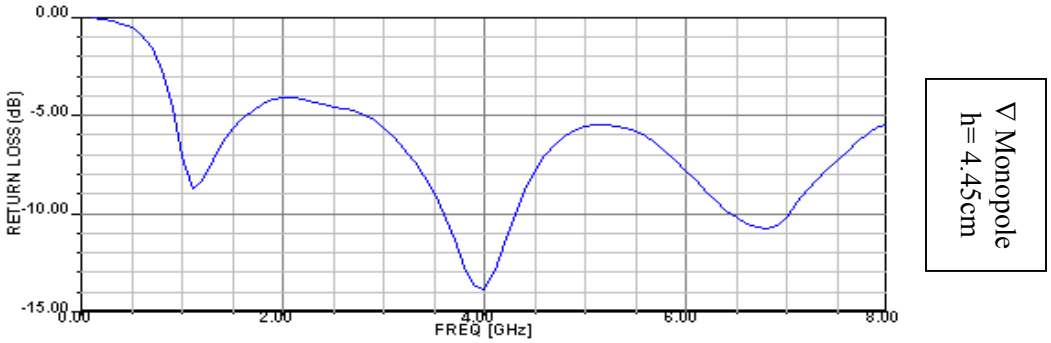

(b)

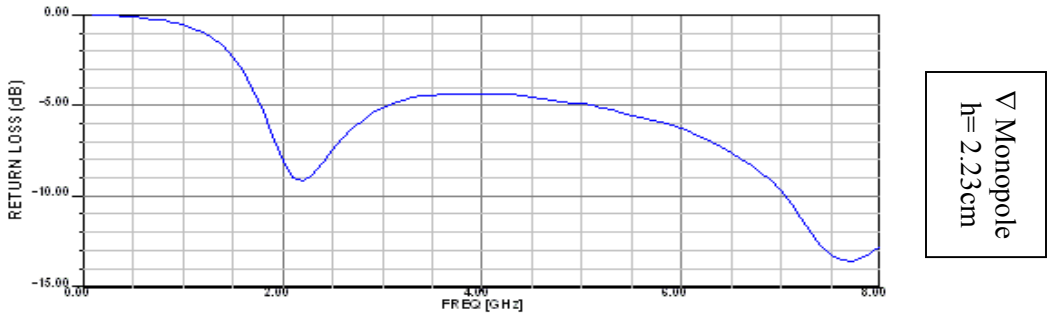

(c)

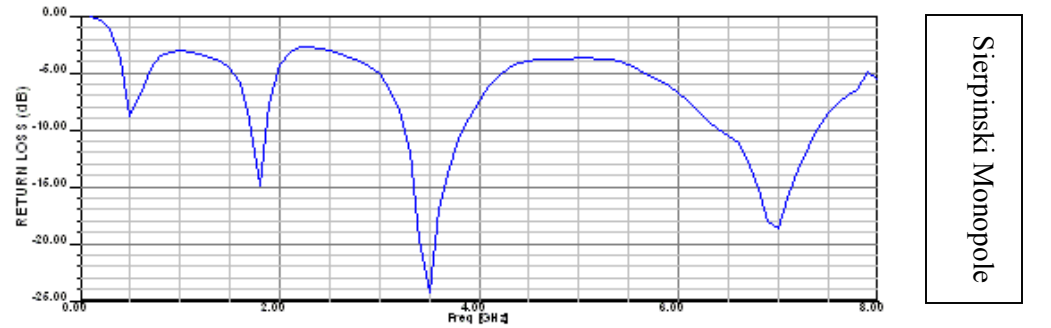

(d)

Figure 3.15: Comparison of return loss of triangular monopoles vs. Sierpinski monopole

Each triangular monopole has the first resonant point at $h/\lambda \approx 0.17$ and also the corresponding higher order modes are periodically spaced (not log-periodically) by a frequency gap of $\nabla f = 0.44\,c/h$ Hz; that is

$$f_n \approx \left(0.17 + 0.44n\right)\frac{c}{h} \tag{3.6}$$

matching the result given in [11].

The second match of the bow tie monopole is always better than the first one, which is clear from the top three plots. Now being well matched than the other bands, we can assume that the second match of the triangular monopole antenna will have a more significant effect on the Sierpinski behavior. Thus comparing the return loss of each of the triangular monopoles to that of the Sierpinski monopole antenna, the bands of the Sierpinski monopole antenna correspond to the second ones of the triangular monopoles. It is noted that the frequency bands of the fractal antenna are slightly shifted towards the origin with respect to the triangular. This slight shift of frequency can be due to the capacitive loading of the upper sub-gaskets because at higher frequencies the active region of the fractal antenna decreases.

The log-periodicity lost in the 1st band of Sierpinski monopole antenna can be explained as: the first band of the Sierpinski antenna appears at the same position as first resonant frequency of the largest triangular monopole antenna because the Sierpinski gasket considered here lacks of larger fractal iterations breaking this way the symmetry with respect to the central bands. Being not appearing at the same position as the first resonant frequency of the largest bow tie monopole and being not the log-periodic one, the first band of the Sierpinski monopole antenna can be termed as the bow tie mode and the three higher log-periodic bands can be termed as the Sierpinski modes.

3.8 Sierpinski Monopole Antenna for WLANS 2.4/5 GHz bands

A multiband antenna based on the Sierpinski Triangle is designed here for a practical application i.e., WLAN bands 2.4 GHz and 5 GHz.

The initial physical parameters of the monopole antenna are derived using the empirical relation given in Eq. 3.5, that is

$$f_n \approx 0.26\frac{c}{h}\delta^n$$

Since $f_n = 2.4GHz$ and $f_{n+1} = 5GHz$, $f_{n+1}/f_n = 2.08 \approx 2$ and hence the scale factor is $\delta = 2$.

Using Eq. 3.5 the initial height of the Sierpinski monopole is calculated. The number of iterations taken is 3. The Sierpinski monopole will resonate at two other frequencies f_0 and f_3, they are simply included to provide continuity so that the truncation effect does not affect the resonant bands of interest.

The final parameters derived after simulation are given in table 3.2.

Physical Parameter	Value
Scale factor, δ	2
Flare angle	60 degree
Height of largest gasket, h	65 mm

Table 3.3: Physical Parameters of Sierpinski monopole for WLAN bands

The monopole antenna based on these parameters is shown in figure 3.16.

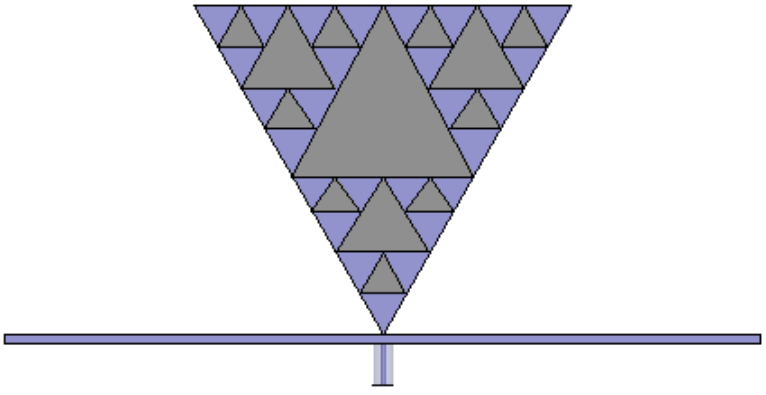

Figure 3.16: Sierpinski monopole for WLAN Bands

3.8.1 Simulated Results of Sierpinski Monopole for WLAN bands

The return loss of the Sierpinski Monopole for Wireless LAN bands is shown in figure 3.17.

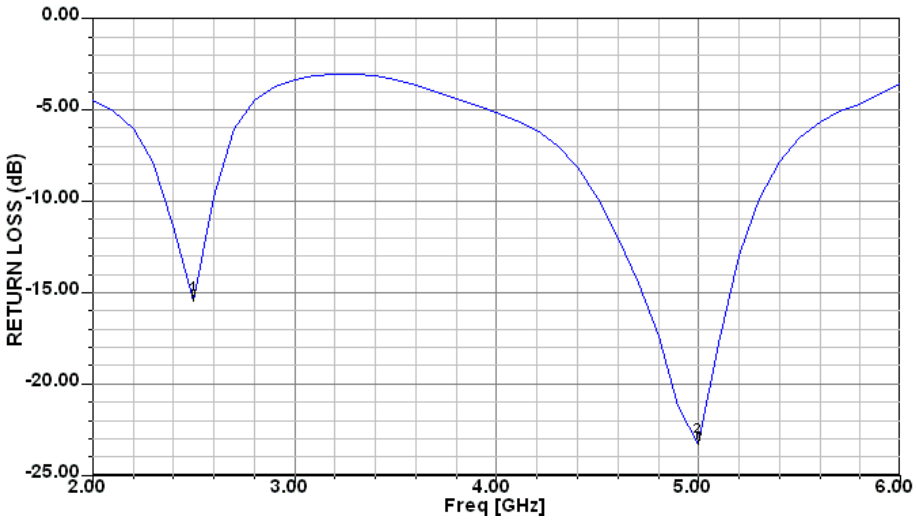

Figure 3.17: Simulated Return Loss of Sierpinski Monopole for WLAN bands

The main cuts of the simulated radiation patterns are shown in the figure 3.18.

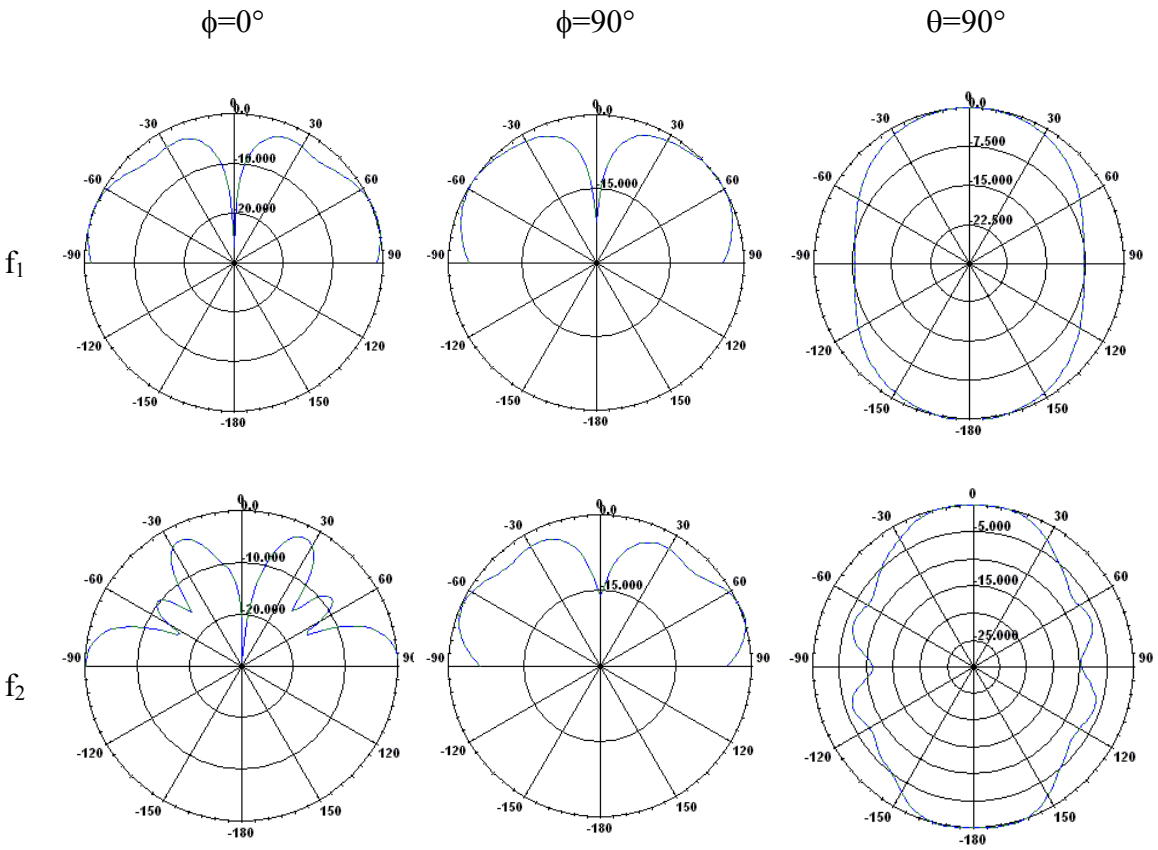

Figure 3.18: Simulated Radiation patterns of Sierpinski Monopole for WLAN bands

CHAPTER 4. VARIATIONS OF THE CLASSICAL SIERPINSKI FRACTAL MONOPOLE

4.1 Introduction

This chapter deals with the different variations of the classical Sierpinski fractal monopole antenna. There are different variations of the Sierpinski fractal possible. Some of these are:

(1) Scale factor variation
(2) Flare angle variation
(3) Self-scalable Sierpinski geometry

We will consider only the scale factor variation and the self-scalable Sierpinski geometry. The classical Sierpinski geometry has a scale factor of two and the monopole antenna based on this geometry as introduced in [10] and discussed in chapter 2 displayed a log-periodic behavior with a log-period equal to the same scale factor that is 2. After exploration of the fact in [10] that the self-similarity properties of the Sierpinski fractal have been translated into the electromagnetic behavior, further research was carried out on the Sierpinski fractal geometry as antenna by changing the scale factor in [13].
It also seems interesting to consider the behavior Sierpinski Geometry with only the center triangles removed and the side triangles not removed.

4.2 Self-scalable Sierpinski fractal monopole (Parany) antenna

4.2.1 Geometry Generation

An equilateral triangle is taken and a central inverted triangle is removed from the parent triangle. As a result, three half-scaled triangles are obtained. In the next stage, a central inverted triangle is removed only form the bottom triangle and so on, this process is repeated on the bottom triangles till the third stage.

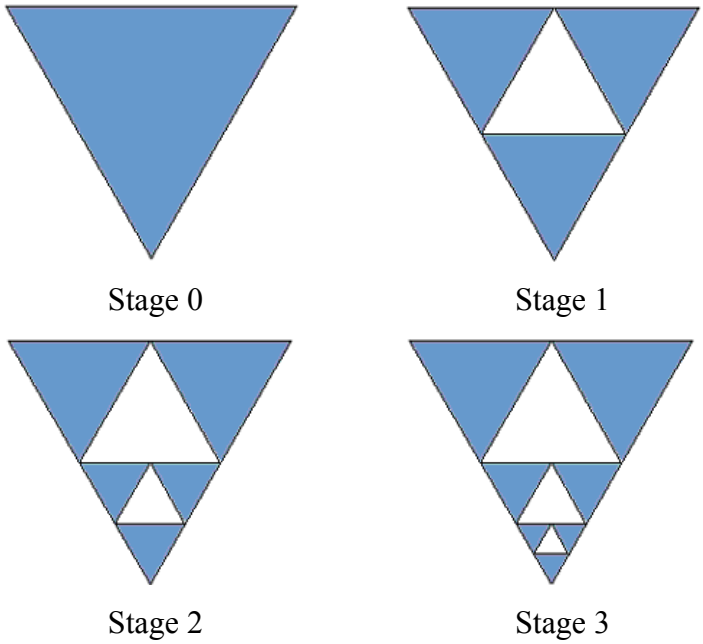

Figure 4.1: Self-scalable Sierpinski Generation

The resulting geometry obtained in figure 4.1 is not a self-similar geometry but instead it is a self-scalable geometry. Also it is not fractal geometry. It should be noted that this geometry appears self-scalable not on a continuous range of scales but only when the proper scale factor ($\delta = 2$) is taken.

4.2.2 Antenna Description

The antenna based on the self-scalable geometry shown in figure 4.2, is of the same height as that of Sierpinski monopole antenna considered in chapter 2 and has a 300 by 300 mm^2 square ground plane as shown in figure. A 50 Ohm coaxial cable modeled in the software feeds the antenna. The antenna has been simulated using Ansoft HFSS.

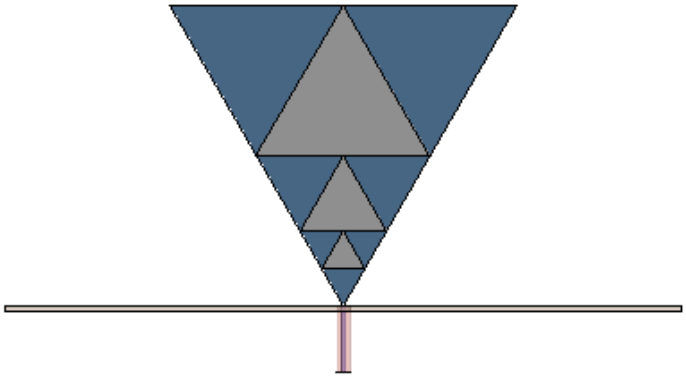

Figure 4.2: Parany Antenna

4.2.3 Input Return Loss of Parany Antenna

The simulated results for the input return loss of self-scalable Sierpinski monopole antenna as well as that of the classical Sierpinski monopole antenna are plotted in figure 4.3. The plot clearly shows a behavior similar to that of the classical Sierpinski monopole antenna, which confirms that the main role in the translation of the geometry properties into the electromagnetic behavior is played by center- removed-triangles. The plot shows a log-periodic behavior with a log-period ($\delta = 2$), except the first band due to the truncation effect again.

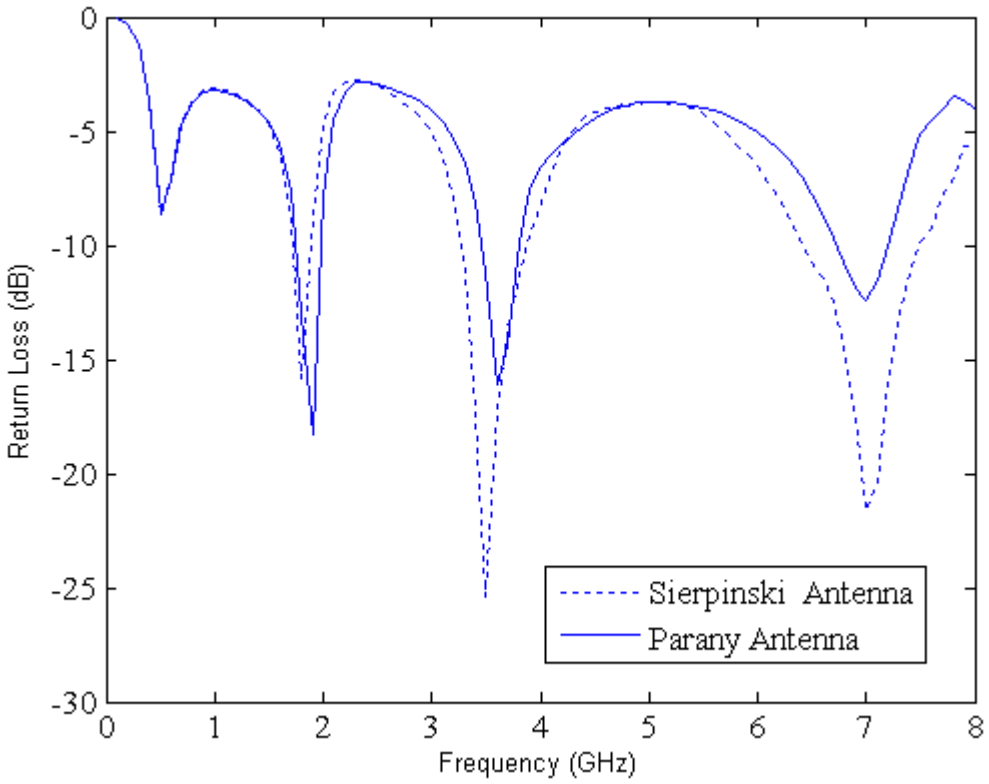

Figure 4.3: Simulated Return Loss of Parany Antenna vs. Sierpinski Antenna

At low frequencies (large wavelengths), the smallest details have a negligible effect on the antenna behavior that is why the behavior of the self-scalable Sierpinski monopole antenna is similar to that of classical Sierpinski monopole antenna at low frequencies as clear from the return loss plots. As the frequency increases, the corresponding wavelength decreases, and the smallest details begins to come in action. The highest band of the self-scalable Sierpinski monopole has a lower bandwidth as compared to that one of the classical Sierpinski monopole. This can be explained as follows: the actual Sierpinski geometry presents many abrupt changes in the current direction as compared to the geometry shown in figure 4.2. And we know that the more the abrupt changes in path of the current flow, the more enhanced will be the radiation. Now Quality factor of an antenna being defined as the ratio of the stored reactive to the radiated power will be decreased and hence bandwidth being inversely proportional to the Quality Factor will be increased. That is why that bandwidth of the highest band of the Sierpinski monopole antenna is greater than that of its counterpart.

4.3 Scale Factor Variation

The classical Sierpinski geometry has a scale factor 'δ' of two, where

$$\delta = h_n / h_{n+1}$$

where 'n' represents the iteration number and 'h' represents the height of the iterated gasket.

Note that h_1= h is the height of the largest gasket.

As explored in [10] and explained in chapter 2, the classical Sierpinski monopole antenna has a log-periodic behavior, both in terms of input parameters as well as radiation patterns. The log-period has a scale factor of 2, the same scale factor that characterized the geometrical self-similarity properties of the fractal object. After this exploration, further research was carried out in [13] on varying the scale factor of the classical Sierpinski and it was found that scale factor variation could allow control of the band spacing.

In the next section we will consider the design and simulation of the antenna based on the Sierpinski geometry with a scale factor of 1.5 as given in [13].

4.3.1 Geometry Generation

The perturbed Sierpinski geometry is constructed in Ansoft HFSS, in an iterative fashion that basically consists in subtracting a scaled triangle from the original equilateral triangle. At each stage, a reduction factor of 1/1.5 is applied on the remaining triangles and total number three iterations are considered here. This whole procedure of the fractal generation is explained in the figure 4.4.

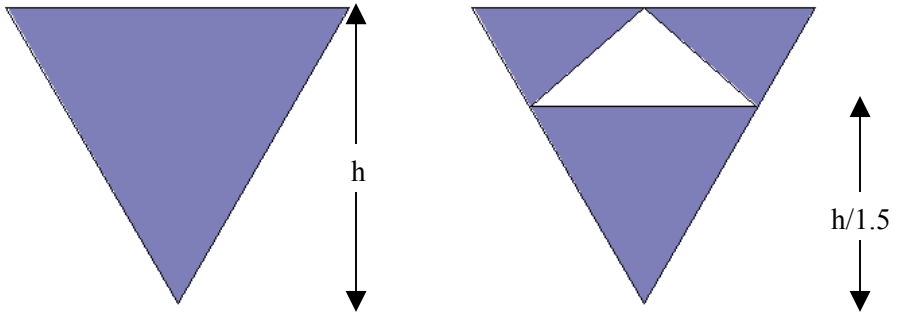

Stage 0 Stage 1

(Contd.)

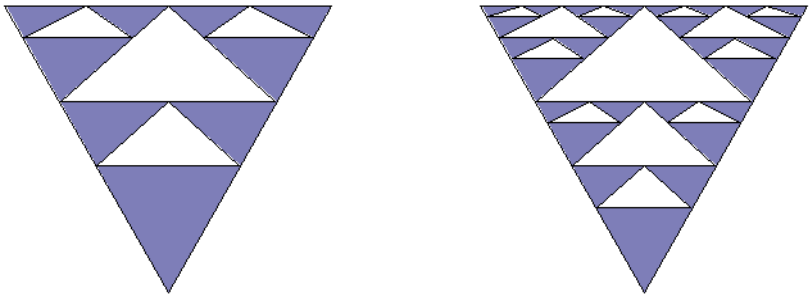

Figure 4.4: Perturbed Sierpinski Fractal Generation

It is clear from the figure that the upper two triangular clusters obtained after each iteration are not the self-similar copies of the overall shape but are rather distorted. Therefore in terms of IFS, an affine transformation rather than a similarity transformation needs to be applied to go from the original equilateral triangle to the final skewed triangles.

4.3.2 Antenna Description

The monopole antenna based on the self-affine geometry has the same description as that of the antenna considered in chapter 2 and is shown in figure 4.5.

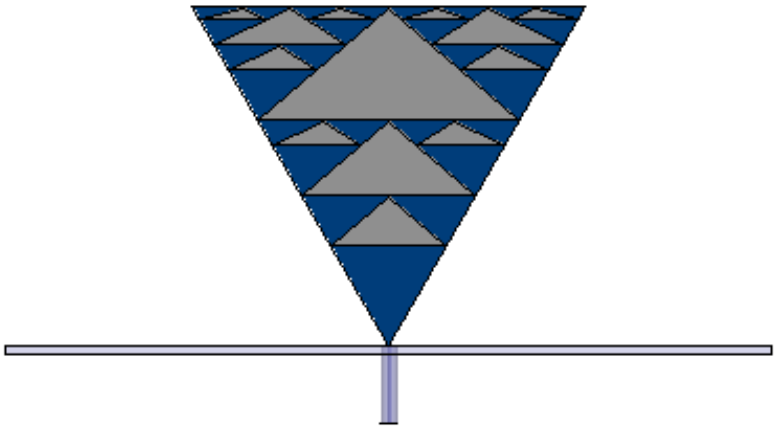

Figure 4.5: Perturbed Sierpinski Antenna with Scale Factor 1.5

4.3.3 Simulated Results of Perturbed Sierpinski Antenna

Input Impedance and Return loss:

The magnitude of the perturbed Sierpinski monopole antenna input reflection coefficient relative to 50 Ohm and the input impedance, both real as well as imaginary parts, obtained from the simulation are shown in the figures 4.6 and 4.7 respectively. For comparison purpose, the simulated return loss of the classical Sierpinski monopole antenna is also given.

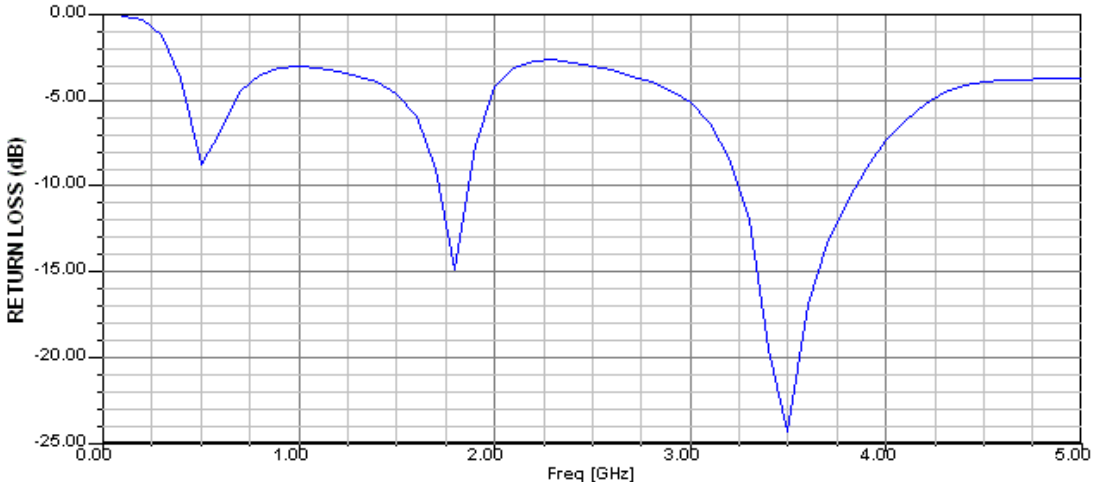

(a)

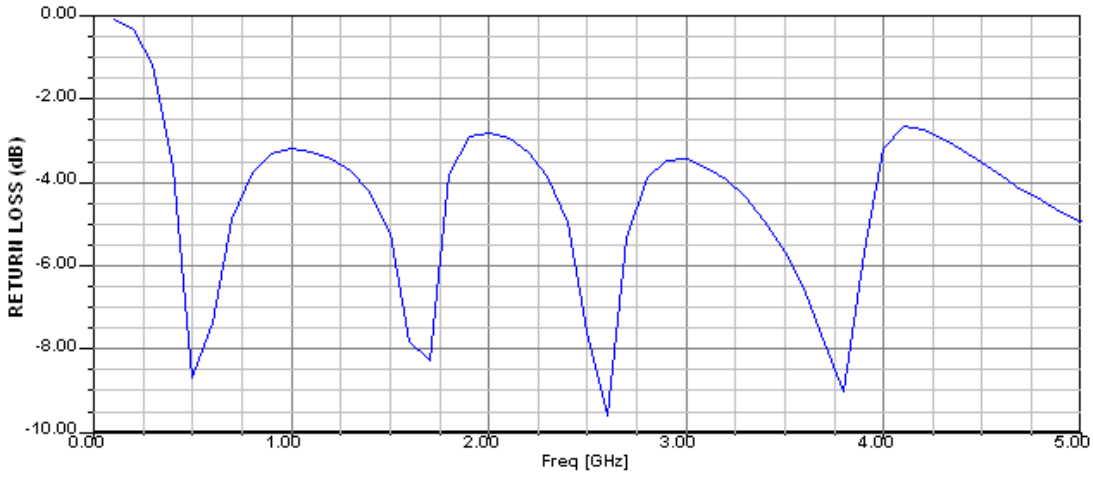

(b)

Figure 4.6: Simulated Return Loss (a)* Classical Sierpinski Monopole (b) Perturbed Sierpinski Monopole

∗NOTE: The frequency axis of the classical Sierpinski is taken up to 5 GHz just for comparison with the Perturbed Sierpinski.

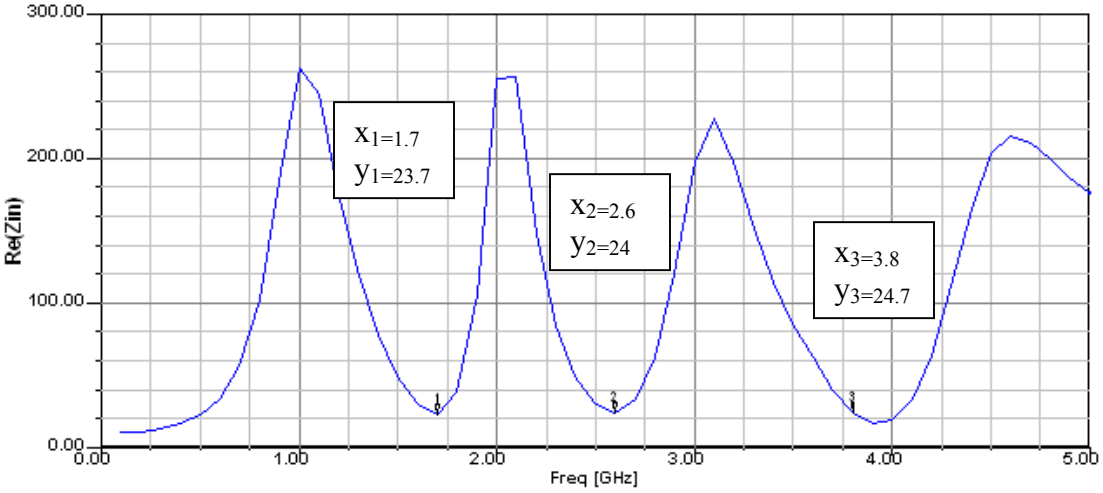

(a)

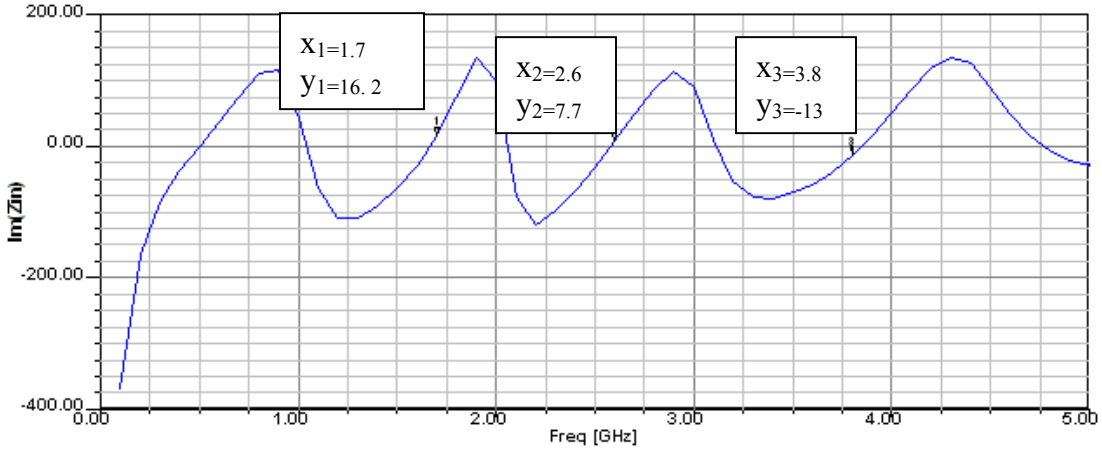

(b)

Figure 4.7: Simulated Input impedance of Perturbed Sierpinski Monopole (a) Real Part (b) Imaginary Part

Band (n)	Frequency (GHz)	Return Loss (dB)	f_{n+1}/f_n
0	0.5	-8.68	3.4
1	1.7	-8.28	1.53
2	2.6	-9.59	1.46
3	3.8	-9.04	-

Table 4.1: Main parameters of the simulated Perturbed Sierpinski Monopole

Once again these plots demonstrate a log-periodic behavior, except the first band, with a log-period 1.5 which is the same scale factor that characterizes the fractal object. These plots also prove that the different bands that are obtained are not just a matter of chance but are spaced according to the scale factor that we choose.

However in comparison to the classical Sierpinski monopole antenna, the bands here are poorly matched which is clear from both the return loss as well as the input impedance of the antenna.

So the following points can be concluded from the so far discussion.

(1) Changing the scale factor allows control of band spacing
(2) Band spacing is controlled at the cost of poor input impedance matching
(3) Irrespective of the scale factor, the first band of the fractal antenna does not follow the log-periodicity due to the truncation effect and it corresponds to the fundamental frequency of the triangular monopole antenna based on the largest gasket.

4.4 Perturbed Sierpinski with microstrip line feeding Technique

The Sierpinski fractal monopole antenna with a scale factor of $\delta = 1.5$ has a log-periodic behavior both in terms of the return loss and the input impedance. But changing the scale factor to change the band allocations results in poor matching characteristics, due primarily to very low resonant resistance.

So it has been established that feeding the perturbed Sierpinski gasket by a coaxial probe through the underside of a large ground plane does not result in an optimum performance and we have to use a feeding scheme that overcomes this problem.

To improve the matching characteristics of the perturbed Sierpinski gasket, microstrip feed technique was used in [14] and we will use the same technique in our case.

A ground plane that is planar with the antenna is introduced as shown in the figure 4.8. The antenna is printed on FR4 substrate ($\varepsilon_r = 4.4$) with standard thickness of 0.5mm and fed at the apex with a 50 Ohm microstrip feed line [15]. This results in modification of the electrical properties from a monopole like configuration to a dipole like configuration and we can assume that the low resistance of the monopole will be increased and will therefore provide better matching characteristics.

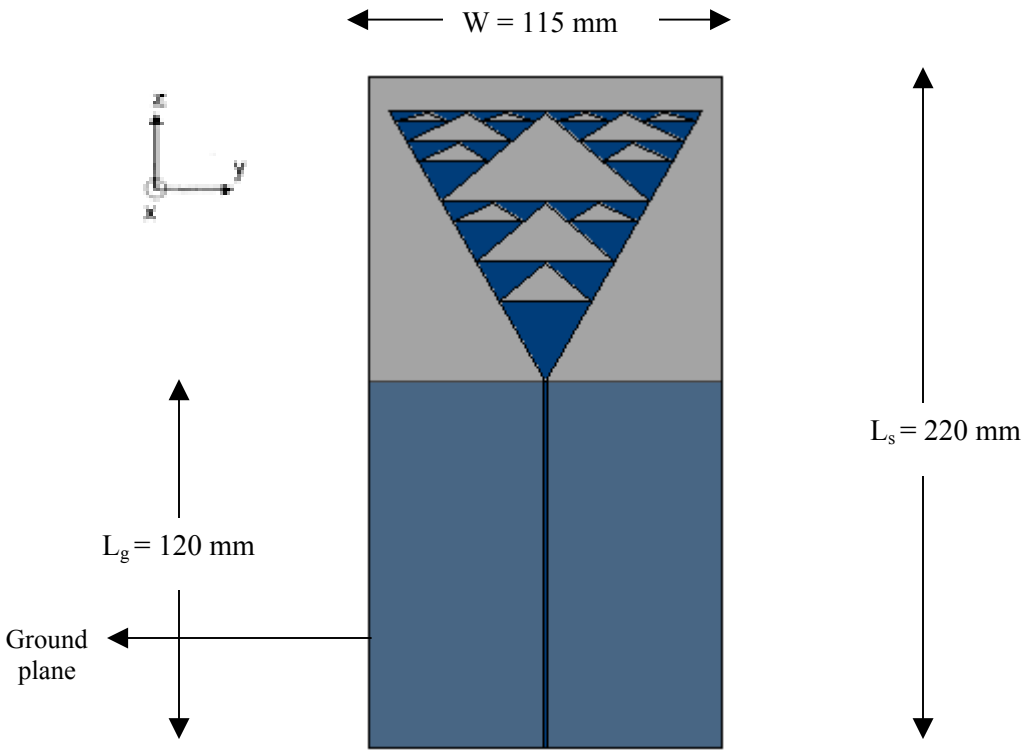

Figure 4.8: Perturbed Sierpinski with microstrip feed

4.4.1 Simulated Return Loss

The simulated result for the input return loss of the perturbed Sierpinski antenna with microstrip feed technique is shown in the figure 4.9.

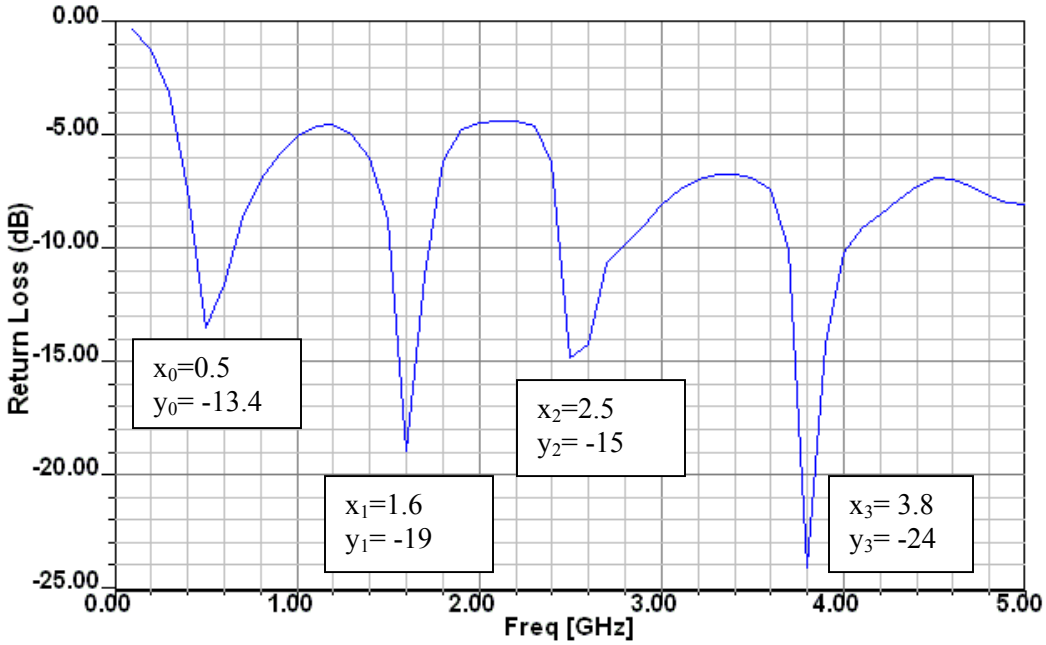

Figure 4.9: Simulated Return Loss of Perturbed Sierpinski Monopole with microstrip feed

The plot shows that all the bands are well matched and the antenna still shows a log-periodic behavior with a log-period equal to the scale factor that characterizes the fractal geometry. As in the previous cases, the first band here also loses the log-periodicity due to truncation effect.

4.4.2 Simulated Radiation Patterns

The radiation patterns of the total electric field of this planar configuration at the three principal plane cuts (ϕ=0°, ϕ=90°, θ=90°) for the three log-periodic bands are depicted in the figure 4.10. The electric field components are normalized with respect to the maximum total electric field value and expressed in dB.

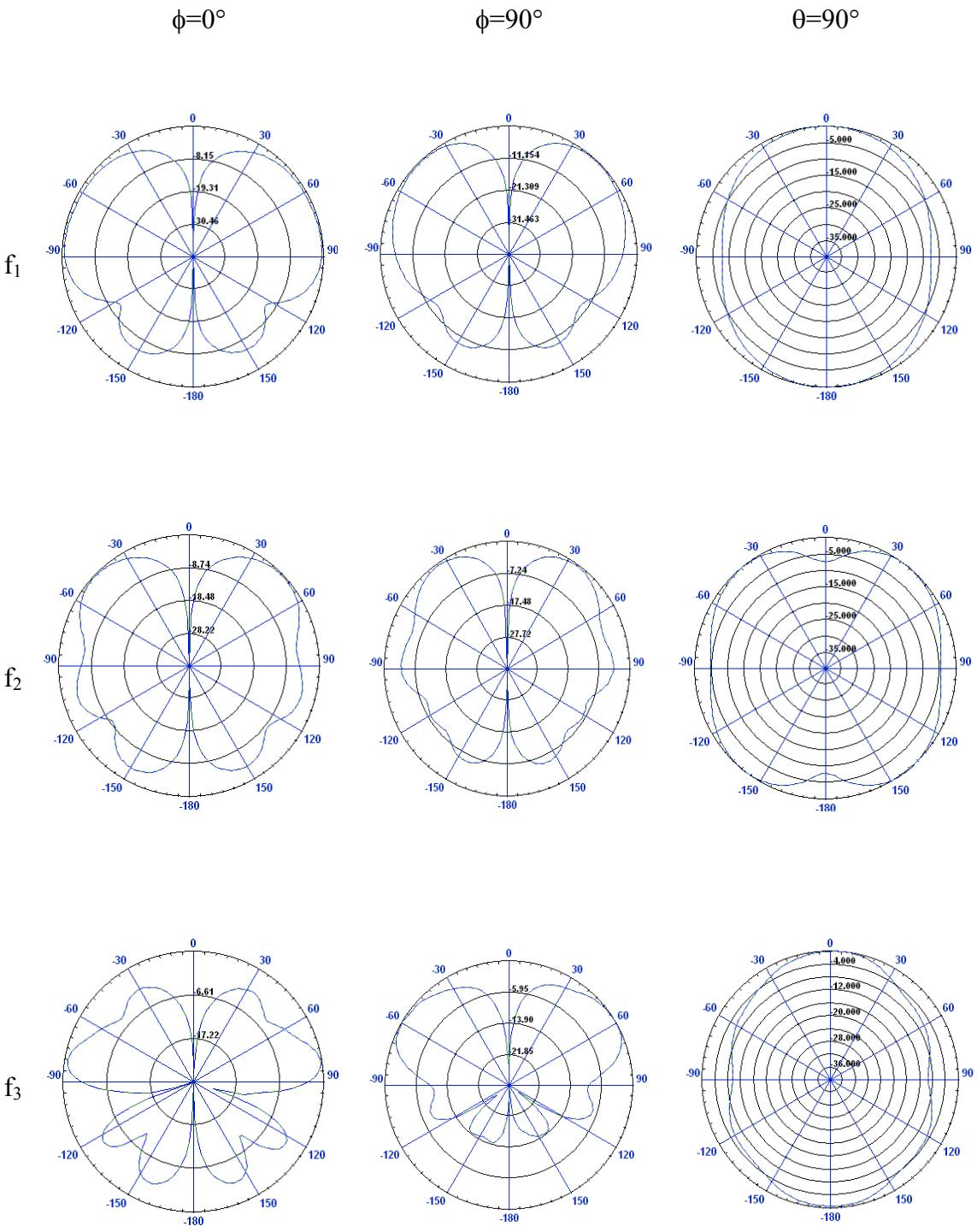

Figure 4.10: Simulated Radiation Patterns of Perturbed Sierpinski Monopole with microstrip feed

The simulated gain of the antenna at the three log-periodic bands is given in the table 4.2. The gain of this planar configuration is lower as compared to the normal ground feed Sierpinski monopole antenna, because of the loss of antenna's image in the perpendicular ground plane [17].

Band	I	II	III
Frequency (GHz)	1.6	2.5	3.8
Gain (dBi)	3	3	4

Table 4.2: Simulated Gain of Perturbed Sierpinski Monopole with microstrip feed

CHAPTER 5. FABRICATION, TESTING AND MEASUREMENTS

5.1 Introduction

In this chapter, fabrication, experimental testing and the measured results of the Sierpinski Monopole antenna and perturbed Sierpinski monopole with microstrip feed designed during this work have been presented. Input reflection coefficient measured using Agilent vector network analyzer PNA E8362B and Far field radiation patterns of the antennas measured using Compact Antenna Test Range (CATR) will be presented.

5.2 Sierpinski Monopole Antenna

5.2.1 Fabrication

The Sierpinski Monopole type antenna is fabricated using LPKF protomat C60, which is a computer controlled precision milling machine. FR-4 substrate (1 mm thick) with single side copper cladding was used for fabrication of the antenna. Actually FR-4 substrate with double side copper cladding was available so one side of the substrate was etched in order to have copper cladding on only one side for final fabrication. The minimum width of the joining sections of the small triangles is taken 0.2mm in order to avoid the breakage of the joints in fabrication.

The antenna was mounted on an aluminum ground plane. A hole was drilled in the ground plane and an SMA connector was used to feed the antenna with coaxial cable.

The characteristic impedance of the coaxial cable is given by

$$Z_0 = \frac{60}{\sqrt{\varepsilon_r}} \ln \frac{D}{d} \tag{5.1}$$

where D is the diameter of the outer conductor and d is the diameter of the inner conductor, ε_r is the dielectric constant of the dielectric between the outer and inner conductor.

The physical parameters of the SMA connector used are given in table 5.1

Physical Parameter	Value
D	4.1mm
d	1.27mm
ε_r (Teflon)	2.1

Table 5.1: Physical Parameters of SMA Connector

The hole to be drilled in the aluminum ground plane was required to be of 4.1 mm diameter but the actual hole drilled is of 4.8mm diameter. So it must be considered when analyzing the results because it will present a discontinuity because of changed impedance.

Two prototypes of the Sierpinski monopole antenna have been fabricated. Figure 5.1 and 5.2 show the snapshots of the two fabricated prototypes of the Sierpinski monopole antenna.

In order to hold the antenna in an upright position on the ground plane, the antenna in prototype1 was adjusted in a packing material (foam) and two L-shaped plastic clips were used on the backside of the packing material with double side tape as shown in figure 5.1.

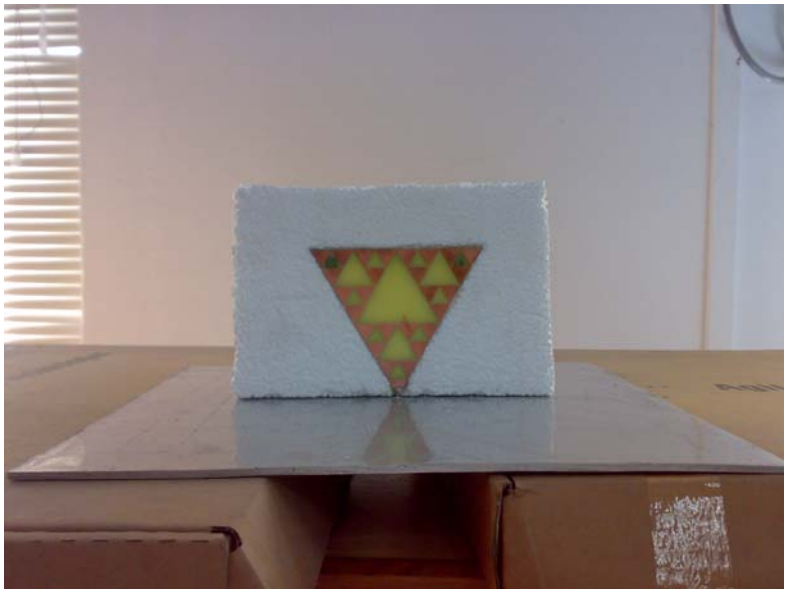

Figure 5.1: Fabricated Sierpinski Monopole Antenna (Prototype1)

Whereas in prototype2, the substrate was extended slightly beyond the radiating structure and two L-shaped plastic clips were used on the backside of the substrate material with double side tape as shown in figure 5.2 in order to give support to the antenna.

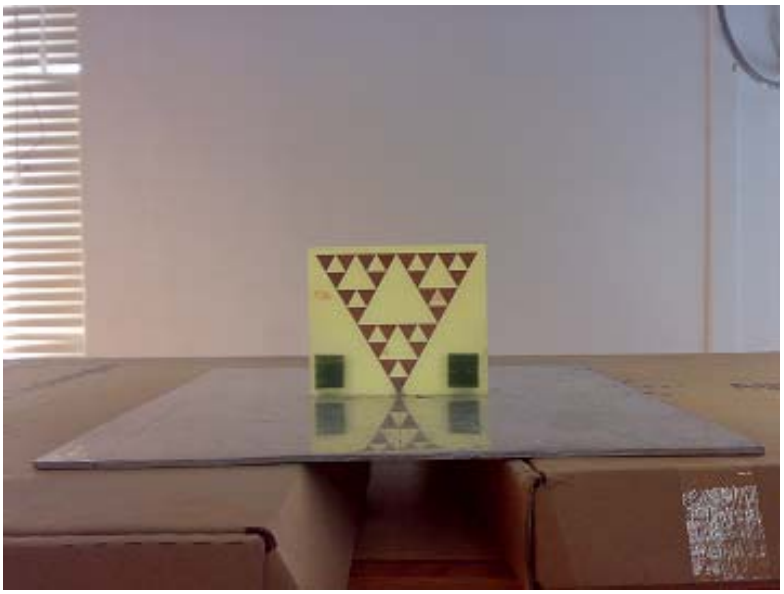

Figure 5.2: Fabricated Sierpinski Monopole Antenna (Prototype2)

5.2.2 Measured Return loss

The measured return loss for the two prototypes of the fabricated Sierpinski monopole antenna is given in figure 5.3 (a, b).

The resonant frequencies of the prototype2 are slightly shifted towards origin as compared to those of the prototype1 because of the larger extension of the dielectric material in prototype2 [20].

(a)

(b)

Figure 5.3: Measured Return loss of Sierpinski Monopole Antenna (a) Prototype1 (b) Prototype2

The main parameters of the Sierpinski monopole antenna derived from the measured return loss are given in table 5.2.

n (Band)	f_n (GHz)	BW (%)	L_r (dB)	f_{n+1} / f_n
1	1.8	10	-12.45	2.04
2	3.67	23	-35	2.05
3	7.51	17	-14	-

Table 5.2: Main parameters of the measured Sierpinski monopole

5.2.3 Measured Radiation Patterns

The main cuts (ϕ=0°, ϕ=90°, θ=90°) of measured radiation patterns of Sierpinski Monopole Antenna at the three log-periodic bands are given in figure 5.4.

The main cuts of the radiation patterns are somewhat similar to each other at the three log-periodic bands. The back lobes in the elevation cuts appear because of the finite ground plane. Also the azimuth cut has an elliptic shape, which means that the antenna radiates strongly in the x-direction because of the larger extension of the antenna in the yz-plane.

The measured gain of the antenna at three log-periodic bands is given in the table 5.3.

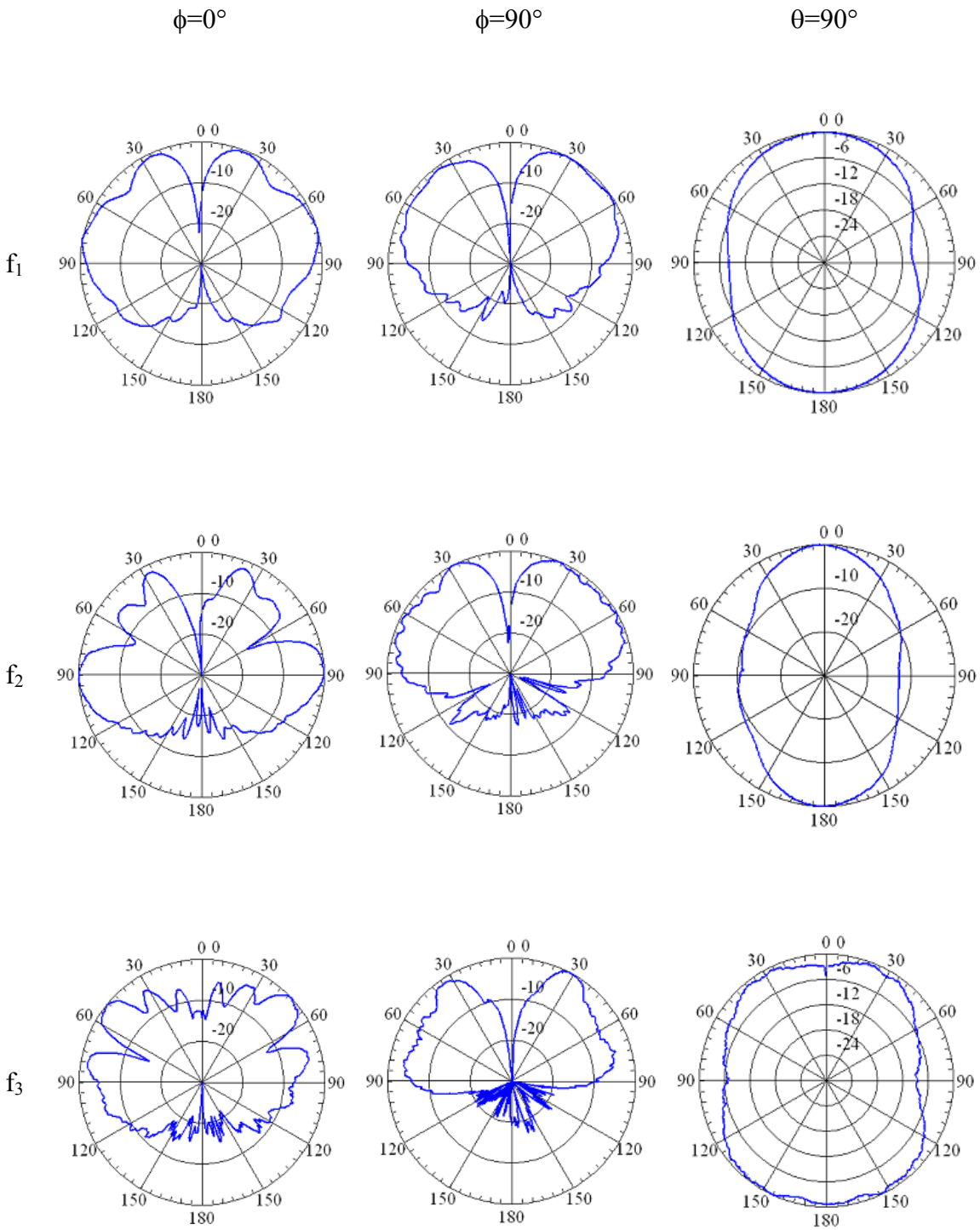

Figure 5.4: Measured Radiation Patterns of Sierpinski Monopole Antenna

Band	Gain (dBi)
I	4.9
II	6.6
III	7

Table 5.3: Measured Gain of Sierpinski Monopole Antenna

5.3 Perturbed Sierpinski with microstrip feed

5.3.1 Fabrication

The Perturbed Sierpinski monopole with microstrip feed is fabricated by Smart PCBs using chemical etching technique. FR4 substrate (0.5mm thick) with double side copper cladding is used here. But it must be noted that the copper cladding on the backside of the radiating structure is removed and it remains only just on the backside of the microstrip line. A 50 Ohm SMA connector is used to feed the antenna with coaxial cable. Figure 5.5 shows the snapshot of the fabricated Perturbed Sierpinski monopole with microstrip feed.

Figure 5.5: Fabricated Perturbed Sierpinski Antenna with microstrip feed

5.3.2 Measured Return Loss

The return loss of the fabricated Perturbed Sierpinski monopole with microstrip feed is measured using Agilent vector network analyzer PNA E8362B and is given in figure 5.6.

Figure 5.6: Measured Return loss of Perturbed Sierpinski Antenna with microstrip feed

The main parameters of the Perturbed Sierpinski monopole with microstrip feed derived from the measured return loss are given in table 5.4.

Band (n)	Frequency (GHz)	Return Loss (dB)	f_{n+1}/f_n
0	0.5	-30.8	3.2
1	1.6	-36.5	1.56
2	2.5	-21.8	1.52
3	3.8	-18.6	-

Table 5.4: Main parameters of the measured Perturbed Sierpinski monopole

5.3.3 Measured Radiation Patterns

The main cuts (ϕ=0°, ϕ=90°, θ=90°) of the measured radiation patterns of Perturbed Sierpinski Antenna with microstrip feed at the three log-periodic bands are given in figure 5.7.

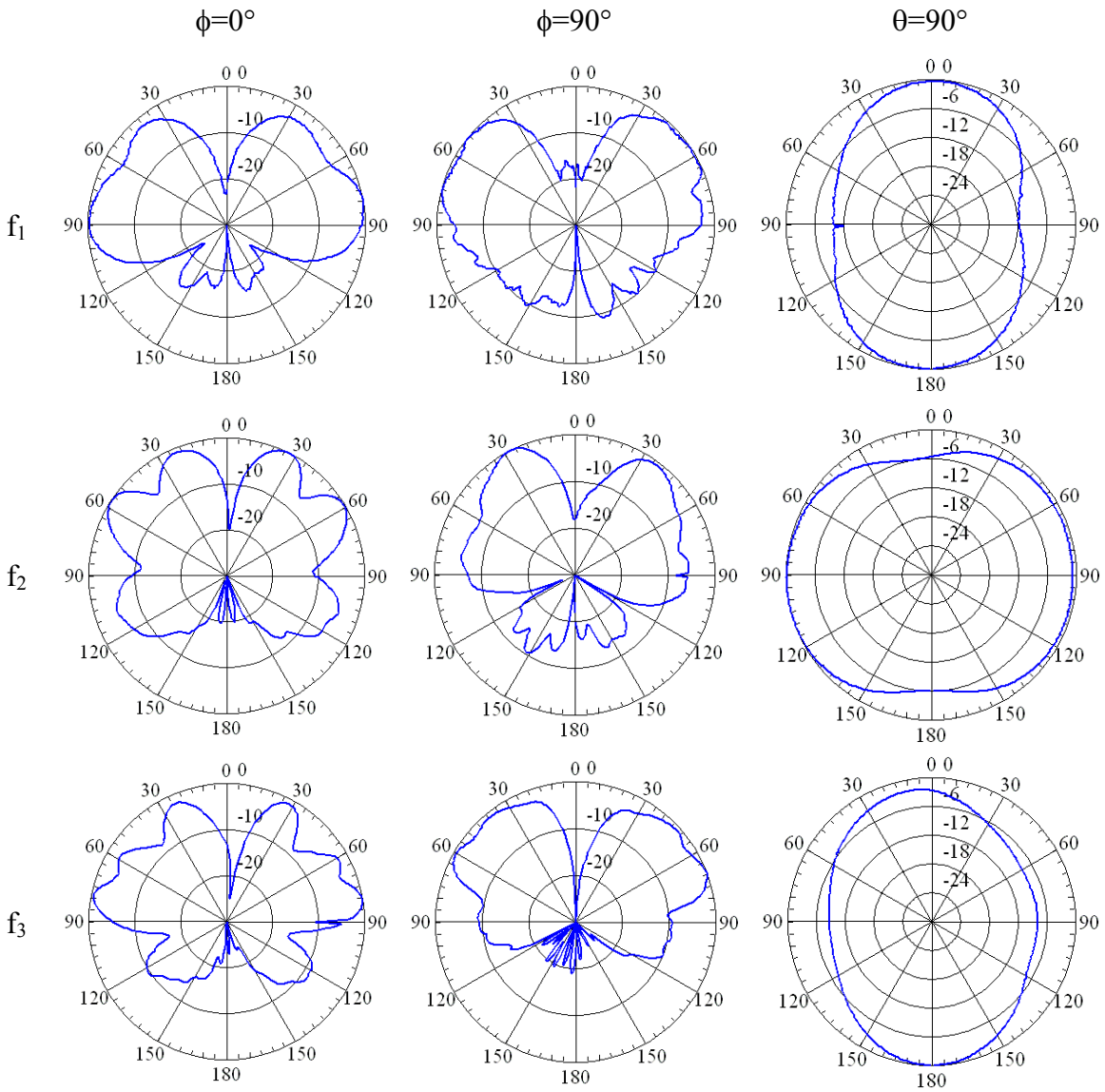

Figure 5.7: Measured Radiation Patterns of Perturbed Sierpinski Monopole fed with microstrip line

The main cuts of the radiation patterns are almost similar at the three log-periodic bands, confirming thus the multiband behavior of the antenna. The azimuth cut (θ=90°) in this case also has an elliptic shape with stronger radiation toward the x-axis.

The measured gain of the antenna at three log-periodic bands is given in table 5.5.

Band	Gain (dBi)
I	6.2
II	1.7
III	2

Table 5.5: Measured gain of the Perturbed Sierpinski Antenna with microstrip feed

CHAPTER 6. RESULTS AND DISCUSSIONS

6.1 Introduction

The main aim of this chapter is to compare the simulated results of Sierpinski monopole antenna and Perturbed Sierpinski Monopole Antenna fed with microstrip line presented in chapter 3 and 4 of this thesis with the corresponding measured results given in chapter 5. The accuracy of measured results in comparison with simulated results and possible causes of deviation from the simulated results will be discussed.

6.2 Sierpinski Monopole Antenna

6.2.1 Input Return Loss

The measured return loss of the Sierpinski Monopole antenna is shown in figure 5.3 (a, b). The difference between two of them is that the result in figure 5.3(a) is for prototype1 in which case the dielectric material behind the radiating structure is of the same size as that of the radiating structure whereas the result in figure 5.3(b) is for prototype2 in which case the dielectric material behind the radiating structure is slightly extended beyond the radiating structure. The resonant frequencies of prototype2 are slightly shifted towards origin as compared to those of the prototype1 because of the larger extension of the dielectric material in prototype2 [20] and hence the field lines in this case well face in their path dielectric material along the radiating structure as well as a little bit beyond the radiating structure.

Comparing the measured return loss with the simulated return loss shown in figure 3.6, it is clear that in both cases the higher three bands are log-periodically spaced with a log-period of 2, which is the same scale factor that characterizes the Sierpinski fractal geometry. The log-periodic bands in the measured return loss are not well matched as compared to those of the simulated return loss. This can be attributed to the fact that hole drilled in the ground plane for SMA connector is slightly of larger diameter than the required diameter as already discussed in chapter 5. And hence it might represent a discontinuity to the signal and result in more reflection. There are ripples in the third log-

periodic band of the measured return loss, which can be related to the that fact at such high frequencies there might be some parasitic frequencies, or there might be some problem in the calibration of the Network analyzer. It is also due to this reason that the third band in the measured return loss is shifted slightly above the corresponding band in the simulated return loss.

6.2.2 Radiation Patterns

The simulated and measured radiation patterns of the Sierpinski monopole antenna are shown in figure 6.1 for comparison purpose, solid line represents the measured patterns whereas the dotted line shows the simulated patterns.

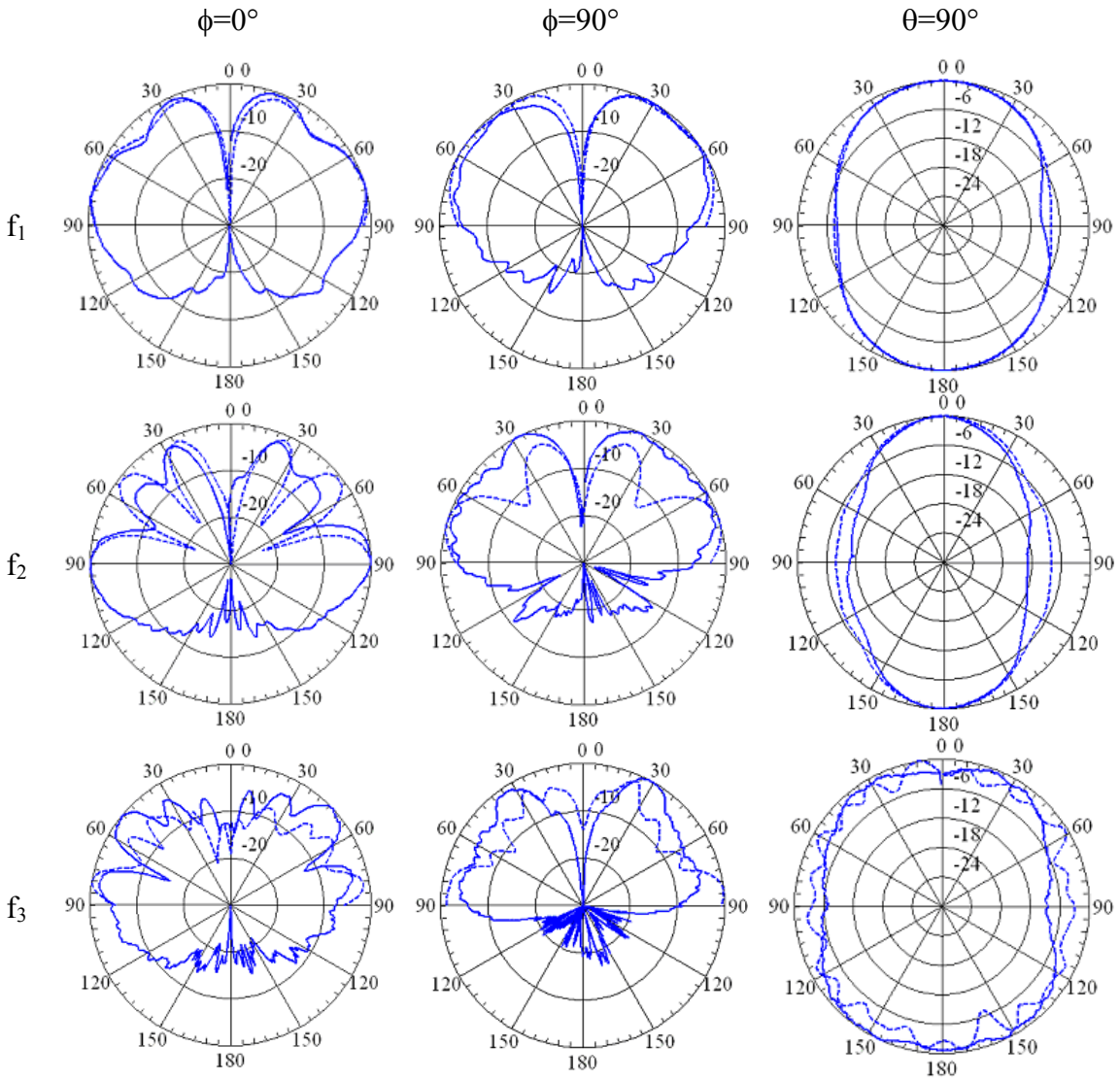

Figure 6.1: Radiation Patterns of Sierpinski Monopole Antenna

Looking at the figure 6.1, we came to know that the main features of the measured radiation patterns are similar to the simulated radiation patterns. One obvious difference between the two is that the measured elevation patterns have back lobes whereas there are no back lobes in the simulated elevation patterns. The main reason for this is that in simulation I have taken the radiation boundary adjacent to the four sides of the square ground plane and hence all the radiation flowing down will be absorbed by the radiation boundary and no back lobes appear in the simulated results.

A comparison between the simulated and measured gain of the antenna at the three log-periodic bands is given in table 6.1.

Band	Gain (dBi)	
	Simulated	Measured
I	5	4.9
II	7	6.6
III	10	7

Table 6.1: Comparison between simulated and measured gain of Sierpinski Monopole Antenna

Looking at the table 6.1, it is clear that the measured gain of the antenna decreases as we go from lower to higher bands, as compared to the simulated gain. This decrease in the measured gain of the antenna at the higher frequencies is due to the fact that the FR4 substrate has a high dielectric loss tangent and the dielectric losses increase with the increase in frequency whereas in simulation Ansoft HFSS assumes a fixed value of dielectric loss tangent. It is due to this reason that FR4 substrate is not suitable for RF designs at high frequencies.

6.3 Perturbed Sierpinski Monopole with microstrip feed

6.3.1 Input Return Loss

The simulated and measured return loss of the Perturbed Sierpinski Monopole Antenna with microstrip feed is given in figures 4.9 and 5.7 respectively. The resonant frequencies in the measured return loss are almost at the same positions as in the simulated result. Both the measured and simulated return loss shows that there are three log-periodic bands spaced with a log-period of 1.5, the same scale factor that characterizes the fractal geometry considered here. The only difference between the two results is that there are some harmonics or ripples in the measured return loss above the 3rd log-periodic band (3.8 GHz). This can be attributed to the fact that in RF design at such high frequencies, there are greater chances of parasitic frequencies to be present as already discussed in the previous section.

6.3.2 Radiation Patterns

The simulated and measured radiation patterns of the Sierpinski monopole antenna are shown in figure 6.2 for comparison purpose. The solid line represents the measured result whereas the dotted line shows the simulated result.

The measured patterns are almost similar to the simulated patterns. Back lobes in the elevation cuts (ϕ=0° & ϕ=90°) are larger as compared to those in the patterns of classical Sierpinski monopole antenna because the Perturbed Sierpinski fed with microstrip line has a planar ground plane. The azimuth cut (θ=90°) clearly shows that the antenna radiates strongly in the x-direction.

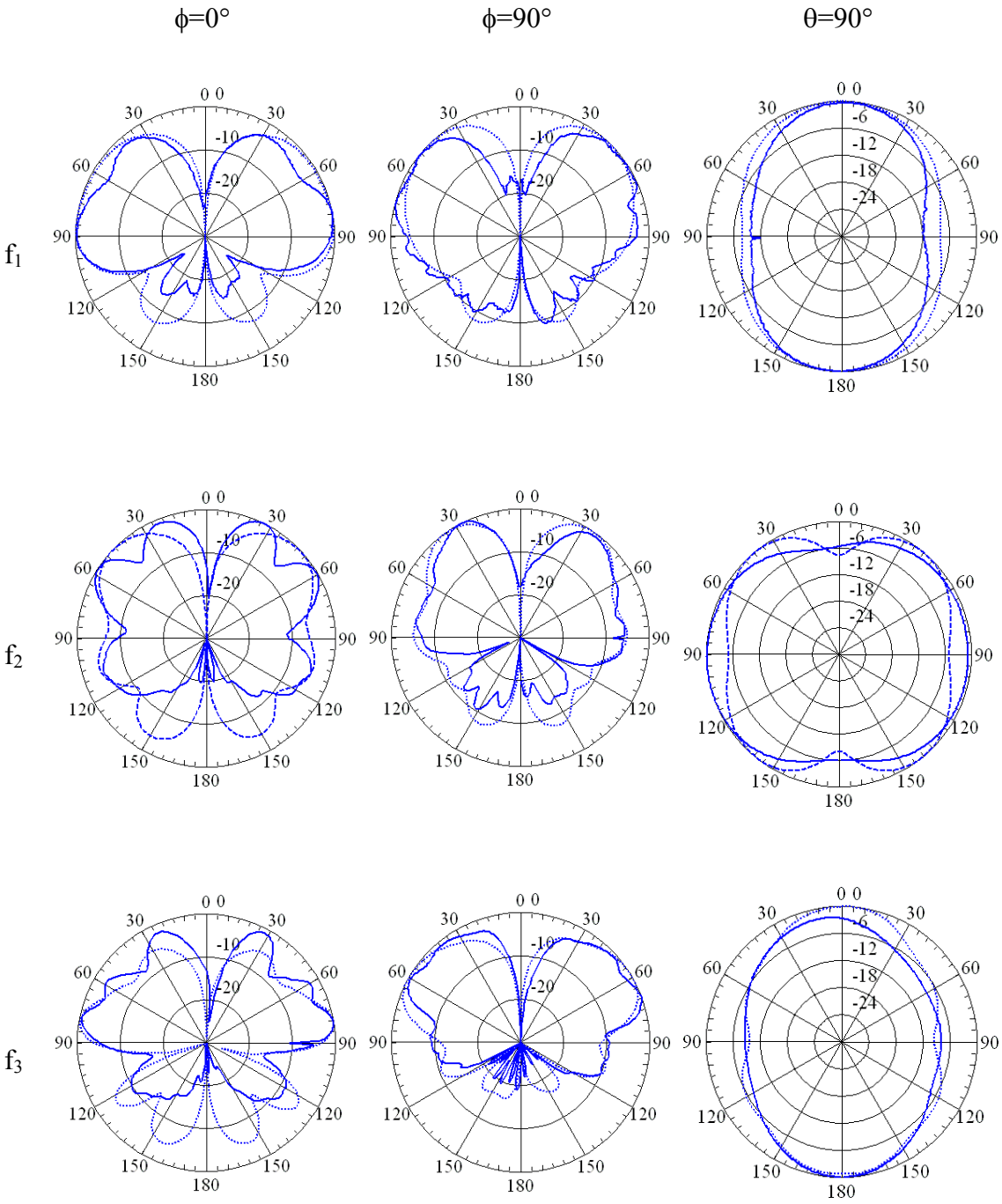

Figure 6.2: Radiation Patterns of Perturbed Sierpinski monopole with microstrip feed

A comparison between the measured and simulated gain of the antenna at the three log-periodic bands, spaced by a factor of 1.5 are given in table 6.2.

Band	Gain (dBi)	
	Simulated	Measured
I	3	6.2
II	3	1.7
III	4	2

Table 6.2: Simulated and Measured gain of Perturbed Sierpinski with microstrip feed

The overall gain of the Perturbed Sierpinski fed with microstrip line is small as compared to that of the classical Sierpinski monopole antenna. This is due to the fact that any radiation directed towards the ground plane in the classical Sierpinski monopole antenna is reflected into the upper half space hence enhancing radiation in the upper hemisphere whereas there is no such ground plane in Perturbed Sierpinski monopole.

CONCLUSIONS

Based on the previous literature, a multiband antenna using the Sierpinski Fractal geometry constructed with three iterations is designed, simulated, fabricated and finally tested. The measured results are in good analogy with the simulated results. The results clearly displayed a multiband behavior with frequencies that are log-periodically spaced by a factor of 2, the same scale factor that characterizes the Sierpinski fractal geometry, confirming the fact that the geometrical self-similarity property of the fractal can be translated into its electromagnetic behavior. The Sierpinski Fractal has been constructed through three iterations and there are three log-periodic bands, hence the number of bands can be controlled with the number of fractal iterations, keeping in view the fabrication issues. To get a sound understanding of the multiband behavior of the Sierpinski Fractal Monopole Antenna, three triangular antennas are simulated and their results are compared with those of the Sierpinski Monopole Antenna. Based on the empirical relation derived from the return loss of Sierpinski Monopole Antenna, a Sierpinski Monopole Antenna for Wireless LAN bands (2.4 and 5 GHz) is designed and simulated.

The geometric scale factor of the Sierpinski fractal is changed from 2 to 1.5 and the simulation of the monopole antenna based on this Perturbed Sierpinski fractal confirmed that changing the scale factor allows the control of band spacing but with a drawback of poor input matching. This poor input matching was rectified with a microstrip feeding scheme instead of feeding the antenna with a coaxial cable down through the ground plane. This final structure of the Perturbed Sierpinski Monopole with microstrip feed was simulated, fabricated and the measured results showed good matching. The resonant frequencies are exactly spaced according to the new scale factor i.e. 1.5.

FUTURE RECOMMENDATIONS

As a practical implementation step in an application, the Sierpinski Monopole Antenna should be mounted on the roof of a car and its behavior should be studied. In simulations its effect can be approximately considered by using a slightly curved ground plane rather than a flat ground plane.

One scale factor has been used in each of the designs discussed in this thesis at a time that is in one case, scale factor of 2 is used and in the 2^{nd} case, a scale factor of 1.5 is used. In practical applications we might not have desired frequencies spaced by some constant scale factor, so multiple scales needs to be introduced in the triangular geometry and it should be analyzed that the whether the frequencies are spaced according to the multiple scales or not. If they are spaced according to the multiple scales, it will be a great advantage.

We know that a base station antenna for cellular communication consists of a triangular array of dipoles. Now replacing these ordinary dipoles with Sierpinski dipoles in the triangular array, a multiband base station antenna should be built.

REFERENCES

[1] R. M. Crownover**,** *Introduction to Fractals and Chaos*. Boston, MA: Jones & Bartlett, 1995.

[2] H. O. Peitgen, H. Jurgens, and D. Saupe, *Chaos and Fractal: New Frontiers of Science*, 2nd ed., Springer-Verlag, 2004.

[3] D. H. Werner and S. Ganguly, "An overview of fractal antenna engineering research," *IEEE Antennas Propag. Mag.*, vol. 45, no. 1, pp. 38–57, Feb. 2003.

[4] C. Puente, J. Romeu, R. Pous, J. Ramis, and A. Hijazo, "Small but long Koch fractal monopole," *IEE Electron. Lett.*, vol. 34, pp. 9–10, Jan.1998.

[5] C. Puente-Baliarda, J. Romeu, and A. Cardama, "The Koch monopole: A small fractal antenna," *IEEE Trans. Antennas Propag.*, vol. 48, pp. 1773–1781, Nov. 2000.

[6] J. Gianvittorio, "Fractal Antennas: Design, Characterization and Applications," Master Thesis, University of California, Los Angeles, 2000.

[7] Nemanja Poprzen, Mico Gacanovic, " Fractal Antennas: Design, Characteristics And Application," *regular paper*.

[8] M.K. A. Rahim, N. Abdullah, and M.Z A. Abdul Aziz, "Microstrip Sierpinski Carpet Antenna Design," *Asia-Pacific Conference on Applied Electromagnetics Proceedings*, Dec. 20-21, 2005.

[9] N. Abdullah, "Microstrip Sierpinski Carpet Antenna Design," Master Thesis, Faculty of Electrical Engineering, University of Technology Malaysia, March 2005.

[10] C. Puente, J. Romeu, R. Pous, X. Garcia, and F. Benitez, "Fractal multiband antenna based on the Sierpinski gasket," *Electron. Lett*., vol. 32, pp. 1–2, Jan. 1996.

[11] C. Puente-Baliarda, J. Romeu, R. Pous, and A. Cardama, "On the behavior of the Sierpinski multiband fractal antenna," *IEEE Trans. Antennas Propag.*, vol. 46, no. 4, pp. 517–524, Apr. 1998.

[12] G. H. Brown and O. M. Woodward, "Experimentally determined radiation characteristics of conical and triangular antennas," *RCA Rev.,* pp. 425–452, Dec. 1952.

[13] C. Puente, J. Romeu, R. Bartolome, and R. Pous, "Perturbation of the Sierpinski antenna to allocate operating bands," *Electron. Lett.*, vol. 32, pp. 2186–2188, 1996.

[14] C. T. P. Song, P. S. Hall, and H. Ghafouri-Shiraz, "Perturbed Sierpinski multiband fractal antenna with improved feeding technique," *IEEE Trans. Antennas Propag.*, vol. 51, no. 5, pp. 1011–1017, May 2003.

[15] G. Gonzalez, *Microwave Transistor Amplifiers: Analysis and Design*, Prentice Hall Ed., 1984, pp. 67-70

[16] C. A. Balanis, *Advanced Engineering Electromagnetic,* John Wiley and Sons, New York, 1989.

[17] C. A. Balanis, *Antenna Theory Analysis and Design*, 3rd ed., John Wiley & Sons, 2005.

[18] J. L. Volakis, *Antenna Engineering Handbook*, 4th ed. McGraw-Hill Inc., 2007, pp. 33.1-33.26.

[19] R.C. Johnson, H. Jasik, *Antenna Engineering Handbook*, 3rd ed. McGraw-Hill Inc., 1993, pp. 4.26-4.32

[20] A. Rubio, A. Salinas, R. Gomez, and I. Sanchez, "Time-domain analysis of dielectric-coated wire antennas and scatterers," *IEEE Trans. Antennas Propag.*, vol. 42, pp. 815–819, June 1994.